

Scholar@UPRM

Dynamic of TNT photo dissociation studied by femtosecond laser-mass spectroscopy

| | |
|---------------|-------------------------------------------------------------------------------------------------|
| Item Type | Thesis |
| Authors | Osorio Cantillo, Celia M. |
| Download date | 2026-06-10 12:52:17 |
| Link to Item | https://hdl.handle.net/20.500.11801/3799 |

Dynamics of TNT photo dissociation studied by femtosecond laser-mass spectroscopy

by

Celia Maribeth Osorio Cantillo

A thesis submitted in partial fulfillment of the requirements for the degree of

MASTER OF SCIENCE
in
CHEMISTRY

UNIVERSITY OF PUERTO RICO
MAYAGÜEZ CAMPUS
2006

Approved by:

Miguel E. Castro Rosario, PhD
President, Graduate Committee

Date

Samuel P. Hernández Rivera, PhD
Member, Graduate Committee

Date

Gustavo López, PhD
Member, Graduate Committee

Date

Nelson Cardona, PhD
Representative of Graduate Studies

Date

Francis Patrón, PhD
Chairperson of the Department

Date

ABSTRACT

The 2,4,6-trinitrotoluene, (TNT), is a widely used explosive material whose photo-dissociation both as a solid and in solution using light radiation has been previously studied. TNT can be used as suitable molecule to learn about the elementary process involved in photo induced dissociation. Furthermore, results in TNT photochemistry may provide information on sensing schemes for this explosive, which can be extrapolated to the detection of other nitroexplosives. NO_2 and NO are typically associated with the photodegradation of TNT. Thus studies that can establish the kinetic energy distribution of nascent NO_2 and secondary NO have the potential of contributing to selective sensing by adding to a library based on differences in internal energy distribution in photoproducts of nitro explosives.

The purpose of this study is to establish the kinetic energy distribution of NO_2 and NO as a product of photo-fragmentation of neat TNT or and TNT on Ottawa sand using femtosecond laser pulses for molecular dissociation and subsequent mass spectrometry measurements as a function of time. Photolysis experiments on TNT deposits irradiated with 100 femtosecond laser pulses at 400 nm and 266 nm wavelengths were performed. NO_2 and NO were analyzed as key fragments. The obtained data showed that there are slight differences in the NO_2 and NO speeds from TNT crystals and TNT deposited on sand and vapor phase of TNT. Those results indicate that the energetic processes that result in fragments ejection are different in all cases. In conclusion, photo-fragmentation using femtosecond lasers followed by mass spectrometry measurement is a sensitive approach for the kinetic energy distribution establishment of NO/NO_2 fragments; besides, its effectiveness could be enhanced coupling it with another spectroscopic method for trace amounts detection of nitroorganic explosives.

RESUMEN

El 2,4,6-trinitrotolueno, (TNT), es un material explosivo extensamente usado cuya foto-disociación como sólido y en solución usando la radiación por luz ha sido estudiado previamente. TNT se puede utilizar como molécula apropiada para aprender sobre el proceso elemental implicado en la disociación foto-inducida. Además, los resultados de la fotoquímica del TNT pueden proporcionar la información para los esquemas de detección a distancia para este explosivo, los cuales se pueden extrapolar a la detección de otros nitroexplosivos. NO_2 y NO se asocian típicamente a la fotodegradación del TNT. Así estudios que puede establecer la distribución de la energía cinética del NO_2 naciente y del NO secundario, tienen el potencial de contribuir a la detección selectiva agregando a una biblioteca basada en diferencias en la distribución de la energía interna en los fotoproductos de nitroexplosivos.

El propósito de este estudio es establecer la distribución de la energía cinética de NO_2 y NO como producto de la foto-fragmentación del TNT solo o/y de TNT en arena de Ottawa usando los pulsos de un laser de femtosegundos para la disociación molecular y las subsecuentes medidas de espectrometría de masas en función del tiempo. Los experimentos del fotólisis en los depósitos de TNT irradiados con pulsos del laser de 100 femtosegundos en longitudes de onda de 400 nm y 266 nm fueron realizados. NO_2 y NO fueron analizados como fragmentos claves. Los datos obtenidos demostraron que hay diferencias leves en las velocidades del NO_2 y del NO provenientes de los cristales de TNT y TNT depositados en la arena y de la fase vapor del TNT. Esos resultados indican que los procesos energéticos que dan lugar a la eyección de los fragmentos son diferentes en todos los casos. En conclusión, la foto-fragmentación usando laseres de femtosegundo seguidos por medidas de espectrometría de masas es un acercamiento sensible para el establecimiento de la distribución de la energía cinética de los fragmentos NO/NO_2 ; además, su eficacia podría ser realizada acoplado con otro método espectroscópico para la detección de cantidades en trazas de explosivos nitroorgánicos.

Dedicated to my two mothers Himelda and Serafina

ACKNOWLEDGEMENTS

I want to acknowledge my advisor, Dr. Miguel Castro for giving me the opportunity to work with him, for guiding me, give me motivation and support in my work. To Professor Dr, Samuel Hernández Rivera for your time and collaboration. And to Professor Dr. Gustavo López for the assistance provided to my project.

I give to thanks God my strong castle, and to my family and my best friend Lissette in the distance. Also, I want to thank all those wonderful people who I have known in these three last years and that today are my friends, among them to my loved Pedro, They, each one of different form contributed to the fulfillment of this purpose.

Table of Contents

| | |
|------------------------------------------------------------------|-----------|
| ABSTRACT | ii |
| RESUMEN | iii |
| ACKNOWLEDGEMENTS | v |
| TABLE OF CONTENTS | vi |
| TABLE LIST | viii |
| FIGURE LIST | IX |
| 1. INTRODUCTION | 1 |
| 1.1 MOTIVATION | 2 |
| 1.2 LITERATURE REVIEW | 3 |
| 1.3 SUMMARY OF FOLLOWING CHAPTERS | 8 |
| 2. THEORETICAL BACKGROUND | 9 |
| 2.1 PHOTOCHEMISTRY | 9 |
| 2.2 PHOTOFRAGMENTATION | 9 |
| 2.2.1 <i>Photodissociation</i> | 10 |
| 2.2.2 <i>Direct reaction</i> | 12 |
| 2.2.3 <i>Isomerization</i> | 13 |
| 2.2.4 <i>Photoionization</i> | 14 |
| 2.3 PHOTOFRAGMENTATION OF NITROAROMATIC COMPOUNDS | 14 |
| 2.3.1 <i>Breakage of NO₂ Group by Light</i> | 14 |
| 2.4 MASS SPECTROMETRY MS AND QUADRUPOLE MASS SPECTROMETRY QMS | 14 |
| 2.4.1 <i>History of QMS</i> | 15 |
| 2.4.2 <i>QMS Equipment</i> | 16 |
| 2.5 KINETIC ENERGY DISTRIBUTIONS | 18 |
| 2.5.1 <i>The Maxwell and Boltzmann Distributions</i> | 18 |
| 2.5.2 <i>Molecular Speeds</i> | 21 |
| 3. EXPERIMENTAL SECTION | 23 |
| 3.1 DESCRIPTION OF THE EXPERIMENTAL SET-UP | 24 |

| | | |
|-----------|---------------------------------------------------------------------------------------------|-----------|
| 3.1.1 | <i>Laser Fragmentation</i> | 26 |
| 3.1.2 | <i>Power Dependence of Signals from Fragmentation</i> | 27 |
| 4. | RESULTS AND DISCUSSION | 28 |
| 4.1 | MASS SPECTROMETRY MEASUREMENTS OF TNT | 28 |
| 4.2 | LIGHT ABSORPTION BY SOLID TNT | 34 |
| 4.3 | TIME-OF-FLIGHT MEASUREMENTS | 35 |
| 4.3.1 | <i>Raw data: Arrival curves for NO₂ and NO fragments</i> | 37 |
| 4.3.2 | <i>Power Dependence of NO₂ and NO signals</i> | 42 |
| 4.3.3 | <i>Manipulated data: Distribution of kinetic energy for NO₂ and NO fragments</i> | 44 |
| 4.4 | COMPARISON BETWEEN VELOCITIES OF FRAGMENTS AND BOLTZMANN DISTRIBUTION | 54 |
| 5. | CONCLUSIONS AND FUTURE WORK | 55 |
| | REFERENCES | 57 |

Table List

| Tables | Page |
|--------------------------------------------------------------------------------------------------------------------------------------------------------------------------|-------------|
| Table 1. Principal fragmentation channels observed in the femtosecond time-of-flight mass spectra of laser-desorbed trinitrobenzene, trinitrotoluene and trinitrophenol. | 5 |
| Table 2. Principal photo-fragmentation pathways observed for dinitrotoluene | 8 |

Figure List

| Figures | Page |
|---------------------------------------------------------------------------------------------------------------------------------------------------------------------|-------------|
| Figure 1. Femtosecond time-of flight mass spectrum of laser-desorbed trinitrotoluene (TNT). | 4 |
| Figure 2. Time-of-flight mass spectrum of laser-desorbed trinitrobenzene (TNB). | 6 |
| Figure 3. Several pathways to loss of electronic excitation. | 9 |
| Figure 4. Absorption to (a) and unbound state at an energy greater than its dissociation energy, and (b) a bound state. | 11 |
| Figure 5. Potential energy curves for a typical diatomic molecule showing the crossing that leads to predissociation | 12 |
| Figure 6. Components of the quadrupole mass spectrometer. | 16 |
| Figure 7. Schematic representation of the primary components within the QMS analyzer probe. | 17 |
| Figure 8. The Boltzmann distribution and population of states. | 19 |
| Figure 9. The Maxwell distributions of molecular speeds. | 20 |
| Figure 10. The speed distribution for the molecules given by Maxwell velocity distribution. | 21 |
| Figure 11. Schematic representation of the experiments conducted to study the laser UV photo-dissociation of TNT and the quadrupole mass spectroscopy measurements. | 23 |
| Figure 12. Schematic design of Stainless steel high Vacuum Chamber. | 25 |
| Figure 13. Fragmentation pattern of TNT for positive ions | 29 |
| Figure 14a. Q-MS spectrum of laser photofragmented 2,4,6- trinitrotoluene (TNT) using 400nm. | 31 |
| Figure 14b. Detail of Q-MS spectrum of laser photofragmented 2,4,6- trinitrotoluene (TNT) using 400nm. | 31 |

| | |
|----------------------------------------------------------------------------------------------------------------------------|----|
| Figure 14c. Detail of Q-MS spectrum of laser photofragmented 2,4,6- trinitrotoluene (TNT) using 400nm. | 32 |
| Figure 15a. Q-MS spectrum of laser photofragmented 2,4,6- trinitrotoluene (TNT) using 266nm. | 32 |
| Figure 15b. Detail of the Q-MS spectrum of laser photofragmented 2,4,6- trinitrotoluene (TNT) using 266nm. | 33 |
| Figure 15c. Detail of Q-MS spectrum of laser photofragmented 2,4,6- trinitrotoluene (TNT) using 266nm. | 33 |
| Figure 13. UV-Vis absorption spectrum of neat TNT | 35 |
| Figure 17. Pulses of Hurricane Ti:Sapphire laser. | 36 |
| Figure 18. Arrival curve for NO ₂ fragment ejected from TNT using 266nm. | 38 |
| Figure 19. Arrival curve for NO fragment ejected from TNT using 266nm. | 39 |
| Figure 20. Arrival curves for NO ₂ from TNT using 400nm. | 40 |
| Figure 21. Arrival curves for NO ₂ from TNT, 400 nm wavelength | 41 |
| Figure 22. Dependence of high kinetic energy distribution peak intensity of NO on excitation laser power. | 42 |
| Figure 23. Dependence of high kinetic energy distribution peak intensity of NO ₂ on excitation laser power. | 43 |
| Figure 24a. Kinetic energy distribution of NO ₂ from TNT using 266nm. | 44 |
| Figure 24b . Kinetic energy distribution of NO ₂ (in the region from 0 to 2000 m/s) from TNT, 266 nm wavelength | 46 |
| Figure 25a. Kinetic energy distribution of NO from TNT using 266nm. | 47 |
| Figure 25b. Kinetic energy distribution of NO (in the region from 0 to 2000 m/s) from TNT, 266 nm wavelength | 48 |
| Figure 26. Kinetic energy distribution of 89 m/z fragment from TNT using 266nm. | 49 |

| | |
|------------------------------------------------------------------------------------------------------------------------|----|
| Figure 27a. Kinetic energy distribution of NO ₂ from TNT using 400nm. | 50 |
| Figure 27b. Kinetic energy distribution of NO ₂ (in the region from 0 to 2000 m/s) from TNT using 400nm. | 51 |
| Figure 28a. Kinetic energy distribution of NO from TNT using 400nm. | 52 |
| Figure 28b. Kinetic energy distribution of NO (in the region from 0 to 2000 m/s) from TNT using 400nm. | 53 |

1. INTRODUCTION

The redistribution of energy within an excited molecule and photo-generated fragments when dissociation occurs constitutes an important goal of chemical physics. Measurements of energy disposal among the fragments produced when an electronically excited molecule decomposes are one source of information about these processes. If a polyatomic molecule absorbs light with an energy exceeding the dissociation energy of its weakest bond, fragmentation can occur which may result in the formation of excited products.¹

The explosive 2,4,6-trinitrotoluene (TNT) has three NO₂ groups located at positions 2,4, and 6 with respect to a methyl group in a toluene structural framework. The photo-dissociation of TNT, has been investigated before using several techniques such as ultrafast laser ionization,² finding that the use of ultrafast lasers (picosecond, femtosecond and nanosecond lasers) have advantages such as low degree of fragmentation, suitable for multiphoton ionization and remote sensing, which is important in molecular analysis of nitro-explosives in the environment. Laser induced fluorescence (LIF) and resonance enhanced multiphoton ionization (REMPI) techniques take advantage of photo physical processes in TNT and present several advantages for its detection over other non destructive analytical techniques.³

The presented in this thesis focuses on the study of the dynamics of photo dissociation process in the TNT molecule using femtosecond laser pulses for photofragmentation and generation of specific NO₂ and NO fragments and subsequent detection by quadrupole time of flight mass spectrometry of selected fragments. Wavelengths of 400 nm and 266 nm from a femtosecond laser were employed for these measurements. With these wavelengths, TNT is photo-fragmented following a multiphoton process. The experiments trail the understanding of the photochemical processes involved in the laser irradiated nitro explosive materials, such as, the determination of the final velocity distribution of ejected NO₂ and NO characteristic fragments.

1.1 Motivation

The development of analytical methods that permit the design of efficient sensors for the rapid detection and monitoring of traces of powerful explosives as well as buried landmine detection, has become an urgent necessity due to the increasing terrorism that continuously threatens civil and political security. For such reason, the scientific work has focused in finding better, faster and more reliable methods that allow the detection of this type of substances in different environments.

Techniques based on the analysis of the information obtained from irradiated atoms or molecules are currently very attractive because light can be used as a spectroscopic signature that permits the accurately identification of explosives in real time analyses. 2,4,6-

trinitrotoluene -TNT- has interesting optical properties with light absorption taking place in the ultraviolet and visible zones due to the presence of NO_2 group. This fact can be used as an advantage for the exploit of femtosecond laser-based instruments to rapid detection and monitoring explosives .

The main objective of this project is to study the effect of femtosecond laser radiation on TNT molecules and explore its use for environmental detection of nitro explosives. A trickle down of this effort is the establishment of the kinetic energy distribution of nascent photo fragments associated with TNT photodecomposition.

1.2 Literature Review

Nitro-compounds such as trinitrotoluene (TNT) and dinitrotoluene (DNT) are widely used explosive materials whose photo-dissociation both as a solid and vapor phase using light radiation have been roughly studied using laser based techniques. One of them is the ultrafast laser technique, which applies ultrafast lasers, such as those capable of delivering pulses with femtosecond duration, in molecular analysis of the nitro-explosives. All laser-based techniques that are used for explosives photo-dissociation, follow the parent molecule or the resulting characteristic fragments from the molecule after irradiation.

Ledingham, and coworkers⁴ (2002), studied femtosecond time-of-flight mass spectra of solid-phase samples of trinitrobenzene, trinitrotoluene, and trinitrophenol. They achieved sample desorption using the 5ns fourth-harmonic output from a Nd:YAG laser set at 266 nm

and 800 nm laser pulses of 80 fs duration for photoionization of desorbed fragments and/or molecules. This work demonstrated the survival of labile molecules following laser desorption and the ability of ultrafast laser ionization to measure analyte molecular and structure-specific ions of the selected nitroaromatic molecules.

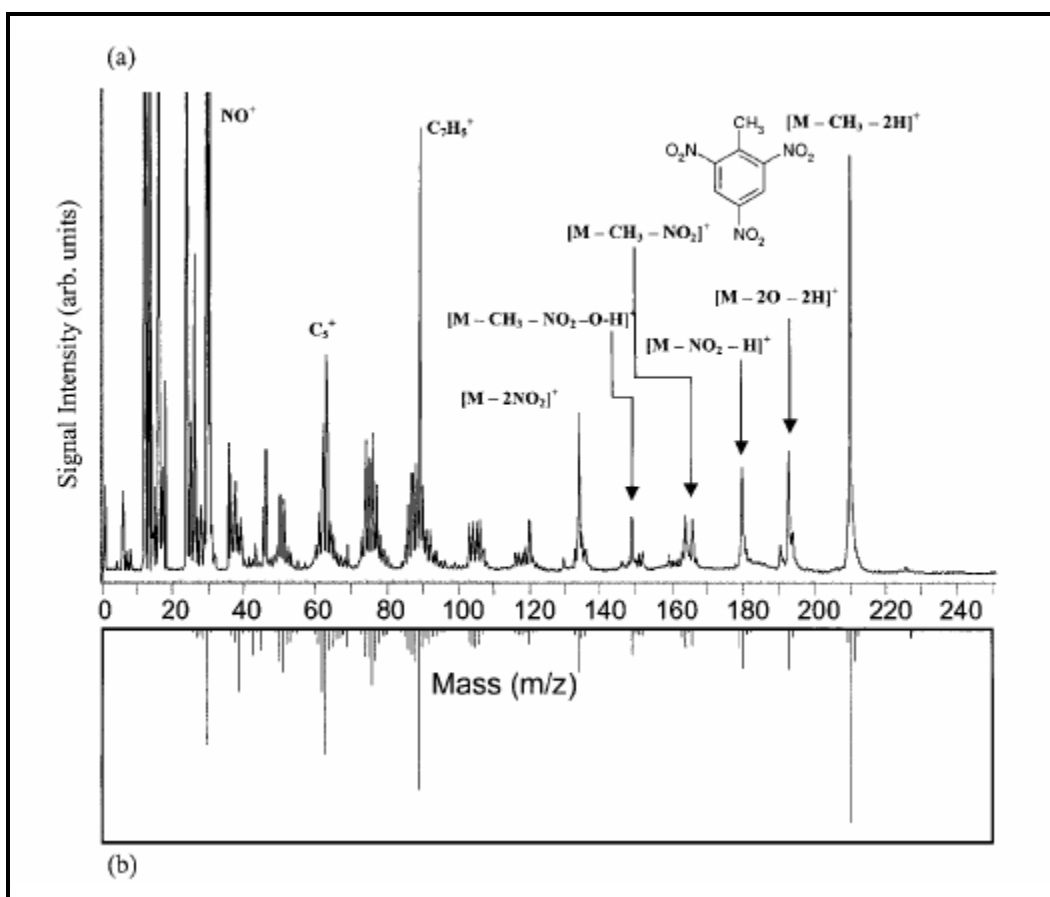


Figure 1. Femtosecond time-of-flight mass spectrum of laser-desorbed trinitrotoluene (TNT). (a) The desorption (5 ns, 266 nm) and ionization (80 fs, 800 nm) laser intensities were 3×10^9 and $6 \times 10^{15} \text{ Wcm}^{-2}$ respectively. (b) EI spectrum at 70 eV. Ledingham, X. et al. *Rapid Commun. Mass Spectrom.* 2002; 16:111-116.

Figure 1 shows femtosecond time-of-flight mass spectrum of laser-desorbed trinitrotoluene (TNT). In the upper part of figure, (a), corresponds to the desorption (5 ns, 266 nm) and

ionization (80 fs, 800 nm) using laser intensities of 3×10^9 and $6 \times 10^{15} \text{ Wcm}^{-2}$, respectively. The spectrum presents the precursor ion and structurally significant ions according to the fragmentation channels shown in table 1. In the low part of figure, (b) the EI spectrum at 70 eV is displayed. Comparing the EI and the laser-induced mass spectra it is clear that they share a number of characteristic features, suggesting that similar processes of molecular fragmentation are occurring. The use of ultrahort pulses guarantees that any fragmentation occurs after ionization and no further absorption of photons by neutral or ionic fragments can occur.⁴

Table 1. principal fragmentation channels observed in the femtosecond time-of-flight mass spectra of laser-desorbed trinitrobenzene, trinitrotoluene and trinitrophenol. Ledingham, X. et al. Rapid Commun. Mass Spectrom. 2002; 16:111-116.

| | |
|--------------------------------------------------------|-------------------------------------------------------------------------------------|
| Trinitrobenzene (TNB) | |
| $\text{C}_6\text{H}_3\text{N}_3\text{O}_6 \rightarrow$ | $\text{C}_6\text{H}_3\text{N}_3\text{O}_5$ (197 Da) + O |
| | $\text{C}_6\text{H}_3\text{N}_2\text{O}_4$ (167 Da) + NO_2 |
| | $\text{C}_6\text{H}_2\text{NO}_2$ (120 Da) + 2NO_2 + H |
| | $\text{C}_6\text{H}_3\text{O}$ (91 Da) + 2NO_2 + NO |
| Trinitrotoluene (TNT) | |
| $\text{C}_7\text{H}_5\text{N}_3\text{O}_6 \rightarrow$ | $\text{C}_6\text{N}_3\text{O}_6$ (210 Da) + CH_3 + 2H |
| | $\text{C}_7\text{H}_3\text{N}_3\text{O}_4$ (193 Da) + 2O + 2H |
| | $\text{C}_7\text{H}_4\text{N}_2\text{O}_4$ (180 Da) + NO_2 + H |
| | $\text{C}_6\text{H}_2\text{N}_2\text{O}_4$ (166 Da) + CH_3 + NO_2 |
| | $\text{C}_6\text{N}_2\text{O}_4$ (164 Da) + CH_3 + NO_2 + 2H |
| | $\text{C}_6\text{HN}_2\text{O}_3$ (149 Da) + CH_3 + NO_2 + H + O |
| | $\text{C}_7\text{H}_5\text{NO}_2$ (135 Da) + 2NO_2 |
| Trinitrophenol (TNP) | |
| $\text{C}_6\text{H}_3\text{N}_3\text{O}_7 \rightarrow$ | $\text{C}_6\text{H}_2\text{N}_3\text{O}_6$ (212 Da) + OH |
| | $\text{C}_6\text{H}_3\text{N}_2\text{O}_6$ (199 Da) + NO |
| | $\text{C}_6\text{H}_3\text{N}_2\text{O}_5$ (183 Da) + NO_2 |
| | $\text{C}_6\text{H}_3\text{N}_2\text{O}_4$ (167 Da) + NO_2 + O |
| | $\text{C}_6\text{H}_3\text{O}$ (91 Da) + 3NO_2 |

Hankin, S.M. and collaborators⁵ (2000), performed studies about ultrafast time-of-flight mass spectrometry using femtosecond ionization of desorbed atoms and molecules. Among those, they analyzed the trinitrobenzene TNB molecule. To carry out this research, they perform the

experiments using a reflectron time-of-flight mass spectrometer and a laser system constituted by a Nd:YAG laser (266 nm, 5 ns, and $1 \times 10^{10} \text{ Wcm}^{-2}$ laser intensity) for laser desorption and an Astra femtosecond laser system (790 nm, 50 fs, and $5 \times 10^{15} \text{ Wcm}^{-2}$ laser intensity).⁵ Particularly for the TNB molecule, they found a significant degree of molecular fragmentation yielding structurally-specific and non-specific fragments. The mass spectrum obtained is shown in figure 2.

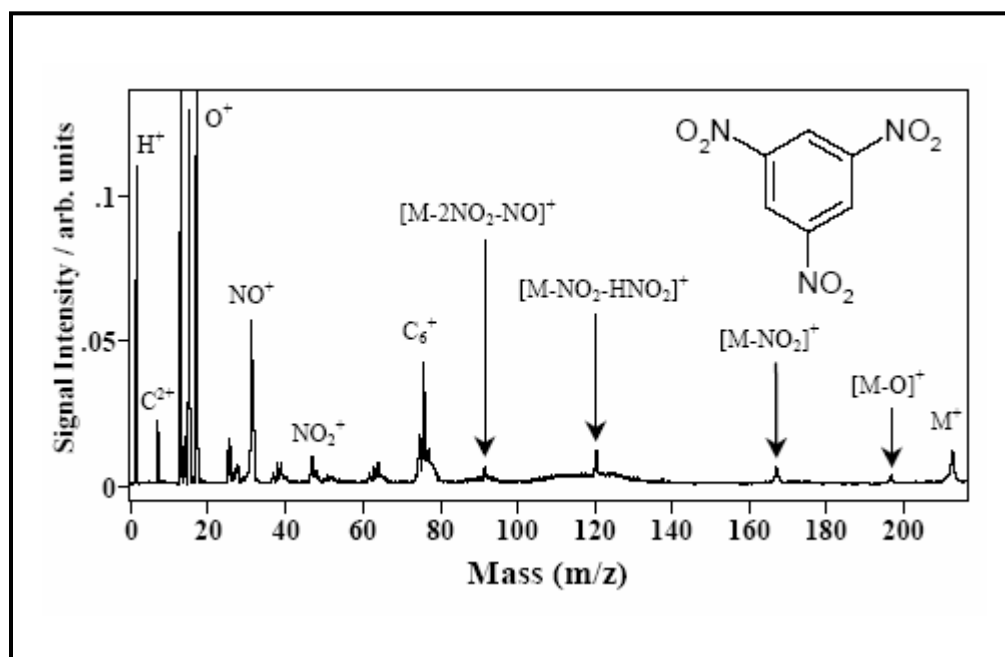


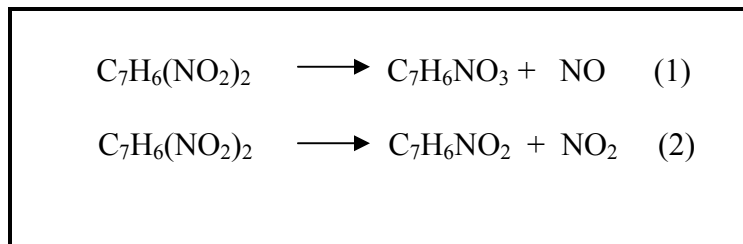
Figure 2. Time-of-flight mass spectrum of laser-desorbed trinitrobenzene (TNB). S. M. Hankin, et al. Science-Astra Laser Programme, Central Laser Facility Annual Report 1999/2000, 89-91.

According to this spectrum, they report $[\text{C}_6\text{H}_3\text{N}_3\text{O}_5]^+$ ($m/z=197$), $[\text{C}_6\text{H}_3\text{N}_2\text{O}_4]^+$ ($m/z=167$), $[\text{C}_6\text{H}_2\text{NO}_2]^+$ ($m/z=120$), $[\text{C}_6\text{H}_3\text{O}]^+$ ($m/z=91$). These ions result from dissociative channels that result in the loss of H, O, NO, and NO_2 from the parent molecule. With this work, they

conclude that the laser desorption and ionization steps play important roles in inducing molecular fragmentation. They also concluded that there is a large kinetic energy distribution in the ions as a result of the desorption event and the energetic fragmentation⁵.

J. Shu, I. Bar, and S. Rosenwaks⁶ (2000), worked in the use of rovibrationally excited NO photofragments as trace nitro-compounds indicators. In this study, they employed one color laser to perform the photolysis of nitrobenzene (NB), and 2,4-dinitrotoluene (DNT), and laser-induced fluorescence to monitor the generated photofragments and detect vapor trace amounts of those nitrocompounds. Those results can be extrapolated to other nitrocompounds, due to the common functional group they have and released in photolysis; that is a characteristic fragment that identifies a class of compounds. Hence, various nitro-compounds eject NO photo-fragments during their photolysis and therefore detection of the latter may indicate presence of the former. To realize the laser photo fragmentation and subsequent laser induced fluorescence LP/LIF, they employed a frequency tripled Nd:YAG laser that pumped a dye laser (Coumarin dye) to produce 440-500 nm. Then this fundamental radiation was frequency doubled by a BBO II crystal to cover 220- 250 nm range of UV radiation (3 ns, 100-1000 μ J). They found in the case of DNT, that NO photofragments may be produced due to photo dissociation of the compound by at least two pathways:⁶ Where the reactions (1) and (2) that are shown in table 2, produce primarily NO and NO₂ products.

Table 2. Principal photo fragmentation pathways observed for dinitrotoluene. Shu, J. et al. Appl. Phys. B, 2000, 70, 621-625.



Hence the formation of NO is important since it serves as a common fragment observed in photo dissociation of many nitrocompounds.⁴ Its identification is aided by the resolution provided by the laser and the typical spectrum obtained. So this method offers the possibility to monitor directly the produced photofragment NO with high sensitivity, but it does not provide selective detection of each different nitrocompound.⁶

1.3 Summary of Following Chapters

We first developed Chapter 1, which includes an introduction, the statement of the objectives as well as a literature review. Following, Chapter 2 deals with the background theory necessary to understand the photochemistry experiments. Subsequently the third chapter presents the methodology and the fourth chapter, presents the results and data analysis. At last, conclusions and future work are presented in Chapter 5.

2 THEORETICAL BACKGROUND

2.1 Photochemistry

The term “photochemistry” is mainly concerned with the chemical changes that are brought about the absorption of light by molecules. However, a number of physical processes that do not involve any overall chemical change lie within the province of the photochemistry.^{7,8}

2.2 Photofragmentation

Photochemical processes involving the absorption of light can be divided into the act of absorption and the subsequent fate of the electronically excited species formed.⁸

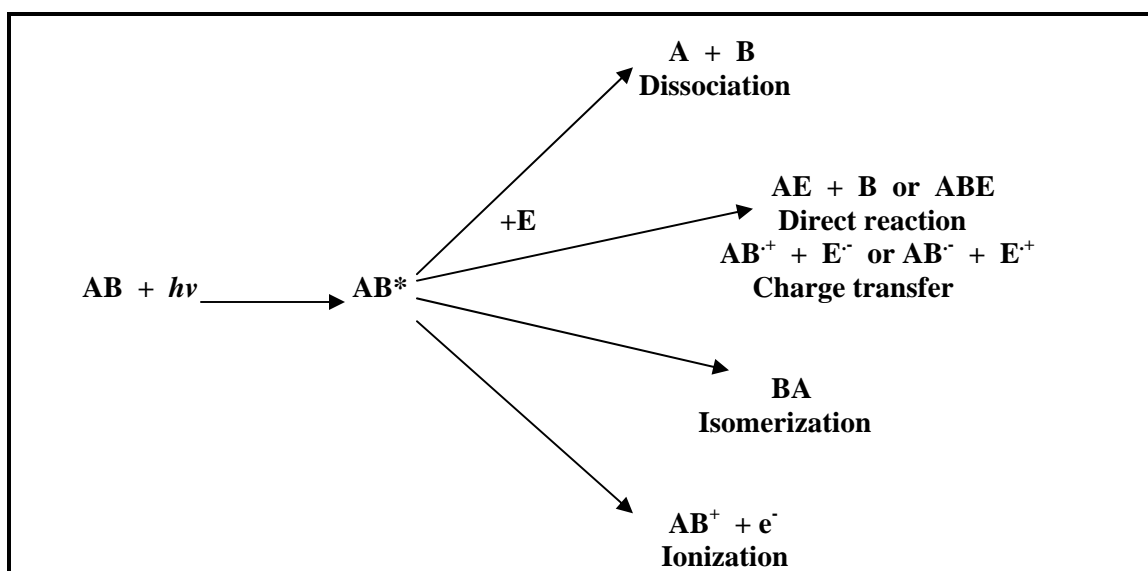


Figure 3. Several pathways to loss of electronic excitation⁸.

As is shown in figure 3 when a molecule has absorbed a quantum of radiation ($h\nu$), becomes 'energy-rich or excited' in the absorption process, and there are several pathways by which an electronically excited species may lose its energy. Among these pathways, some can involve chemical changes and can come about as result of dissociation of the absorbing molecule into reactive fragments or as a result of direct reaction of the electronically excited species; others can result in isomerization process or can conduct to the production of an ion and an electron, like ionization processes.

2.2.1 Photodissociation

The process whereby the excited state species is split into simpler fragments is called photodissociation. However, there are three major routes to photodissociation: optical dissociation, predissociation and induced predissociation. Optical dissociation may come about either if light absorption occurs so that the excited species possesses energy greater than its own dissociation energy, or if the absorption occurs to an unbound, repulsive state. Both cases are shown in figure 4.

The products of an optical dissociation lie upon the same potential surface as the upper state reached by absorption, i.e. the products correlate with the excited state. It is fairly common in optical dissociation for the upper state to correlate with at least one excited fragment, thus leading to one or more excited product fragments being formed.⁸

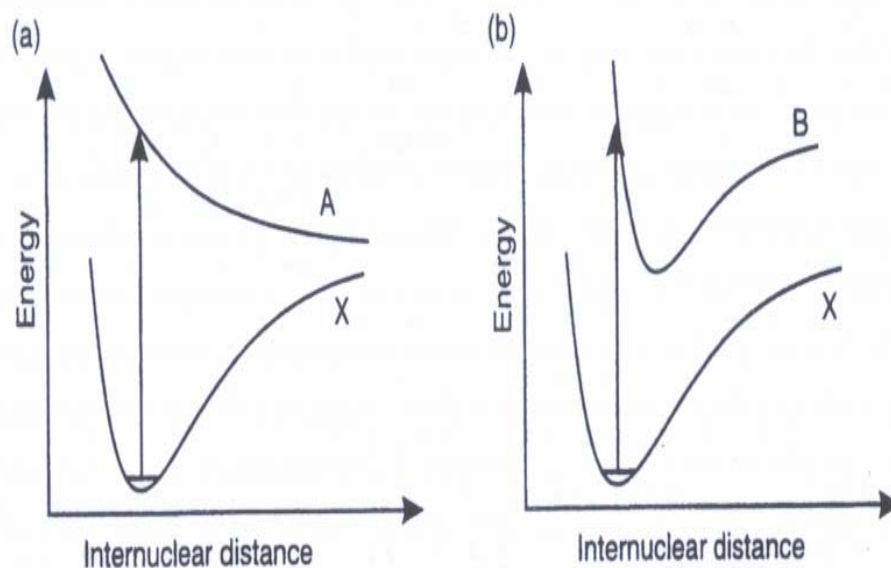


Figure 4. Absorption to (a) an unbound state at an energy greater than its dissociation energy, and (b) a bound state⁸.

When the process involves population of an excited state below its dissociation limit, and subsequent radiationless transition to populate another state above the dissociation limit of that second state, the phenomenon is referred to as predissociation. Figure 5. shows the case of predissociation of a diatomic molecule. Absorption populates the upper bound curve at an energy above where the repulsive curve crosses it. Then the system may cross to the repulsive state, which falls apart to yield the atomic fragments. In a more complex molecule, the sequence of events is essentially the same, with chemical dissociation occurring from a dissociative state at an energy less than that of the state first populated by absorption.

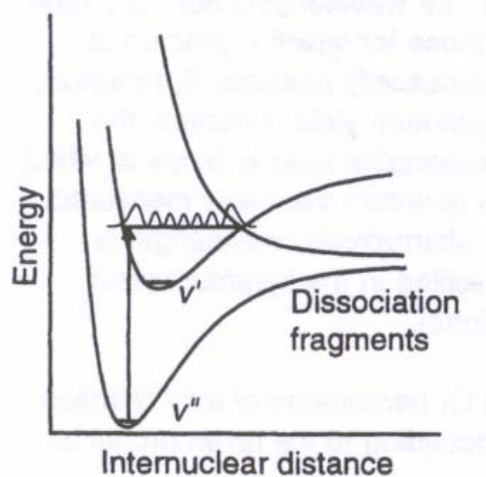
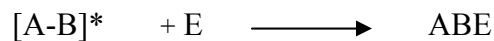


Figure 5. Potential energy curves for a typical diatomic molecule showing the crossing that leads to predissociation.⁸

In certain instances, radiationless transitions that are apparently forbidden by the selection rules can occur in the presence of perturbing influences such as collisions or external electric or magnetic fields. If such radiation less transitions lead to dissociation, the phenomenon is referred to as induced predissociation.

2.2.2 Direct reaction

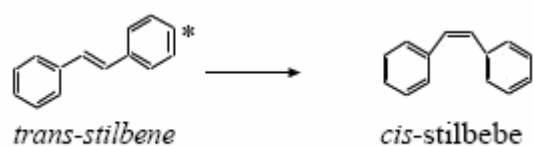
This route represents the situation in which the excitation is used to promote a reaction that is not possible for the ground electronic state.



2.2.3 Isomerization

This phenomenon occurs when photoexcited species may be converted into an isomer. An example of this kind of step is afforded by E-Z (cis-trans) isomerization in which a double

bound in the ground state becomes essentially a single bond about which rotation can occur in an excited state. For example, *trans*-stilbene can be photoexcited to a state that allows free rotation around the alkene's double bond. The photoexcited species is able to relax back to the ground state at any time, and if this happens when the excited stilbene is in the *cis* conformation, ground state *cis*-stilbene will be formed.



2.2.4 Photoionization

Photodetachment of an electron, or photoionization, can be regarded as a special case of photodissociation, with the ion and electron as dissociation products:



This process is of great importance in the upper atmosphere, where short-wavelength ultraviolet radiation from the Sun can lead to appreciable ionization of the chemical species present. It also constitutes the basis of other analytical techniques such as resonance multiphoton ionization.

2.3 Photofragmentation of nitroaromatic compounds

Nitroaromatic compounds such as TNT, interact strongly with UV-Vis radiation and several photochemical processes may be observed. Studies conducted by laser irradiation of solid energetic materials with ultraviolet (UV) light demonstrated the generation of gaseous molecules or fragments that can be detected by mass spectrometry, optical spectroscopy or both³.

2.3.1 Breakage of NO₂ group by light

The functional nitro group, can be considered weakly attached to the nitroaromatic molecules. For example, TNT has a bond dissociation energy for R—NO₂ scission by approximately 60 Kcal/mol.⁹ However, TNT has several alternative decomposition pathways that compete with R—NO₂ bond scission. These pathways also decrease the initial production of NO₂ and contribute to TNT's lower sensitivity relative to other nitrocompounds. As well as, TNT can be photodissociated to NO₂(X²A₁), which absorbs one photon of 266-nm radiation,- a UV photon- and undergoes a transition to the 2²B₂ state. The 2²B₂ state is rapidly predissociated to produce NO.¹⁰

2.4 Mass spectrometry MS and quadrupole mass spectrometry QMS

Since its beginnings about 100 years ago, mass spectrometry (MS) has become a virtually ubiquitous research tool. Scientific breakthroughs made possible by MS have included the discovery of isotopes, the exact determination of atomic weights, the characterization of new

elements, quantitative gas analysis, stable isotope labeling, fast identification of trace pollutants and drugs, and the characterization of molecular structure. The history of MS began with Sir J. J. Thomson of the Cavendish Laboratory at the University of Cambridge, whose studies on electrical discharges in gases led to the discovery of the electron in 1897. In the first decade of the 20th century, Thomson went on to construct the first mass spectrometer (then called a parabola spectrograph) for the determination of mass-to-charge ratios of ions. In this instrument, ions generated in discharge tubes were passed into electric and magnetic fields, which made the ions move through parabolic trajectories. The rays were then detected on a fluorescent screen or photographic plate. Thomson received the 1906 Nobel Prize in Physics “in recognition of the great merits of his theoretical and experimental investigations on the conduction of electricity by gases¹¹. Since Thompson, many different types of mass spectrometers have been developed, among them is the quadrupole mass spectrometer QMS.

2.4.1 History of QMS

One type of mass spectrometer that proved to be ideal for coupling to separation instruments is the quadrupole mass filter, which was first reported in the mid-1950s by the group of physics professor Wolfgang Paul of the University of Bonn, who shared the 1989 Nobel Prize in Physics for his work on ion trapping. In a quadrupole device, a quadrupolar electrical field (comprising radiofrequency and direct-current components) is used to separate

ions. The quadrupole mass spectrometers are fast instruments and have also become very popular as standalone spectrometers. ¹¹

2.4.2 QMS equipment

The analyzer is a specially engineered form of quadrupole mass spectrometer. The total analyzer equipment consists of three sections: the RF generator, the probe, and the control console, see figure 6.

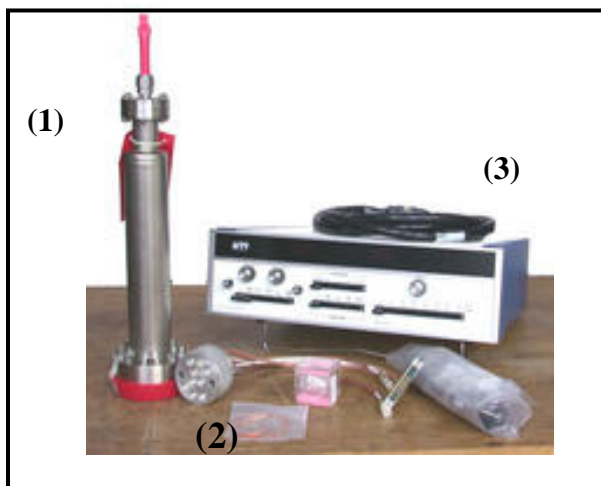


Figure 6. Components of the quadrupole mass spectrometer ¹². (1) probe, (2) RF generator, (3) control console.

The primary components within the analyzer probe are the ionizer, the quadrupole mass filter section, and the ion detector (electron multiplier). A schematic representation is showed in figure 7. These system components are operated to provide mass analysis in the following manner:

- a. Ionization. Gas molecules within the ionizer are bombarded by electrons from the filaments and become positively charged ions, which are then injected into the filter section.
- b. Filtering. Two pairs of metal rods in the filter section form a combined radio frequency and electrostatic field. A charged substance with a specific mass- to-charge ratio will have a dynamically stable trajectory within the field formed by the voltage on the rods; all the other substances will be filtered out. By continuously varying the applied voltages, a range of substances can be sequentially stabilized, and these traverse the length of the filter assembly

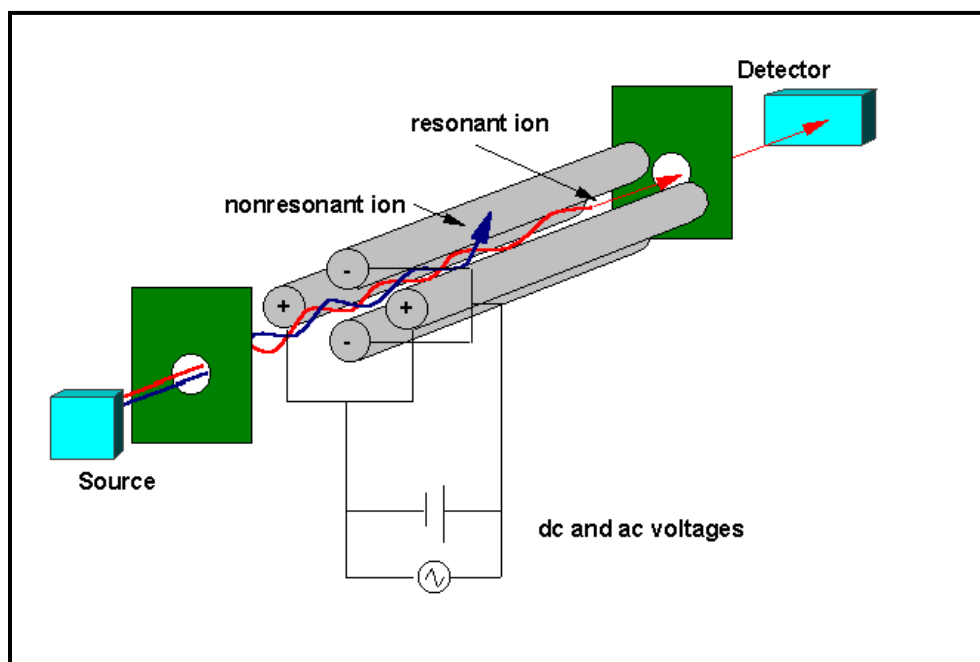


Figure 7. Schematic representation of the primary components within the QMS analyzer probe. (obtained from huygenscms.gsfc.nasa.gov/MS_Analyzer_1.htm, accessed 03/03/06)

c. Detection. The substance traversing the filter is detected by an “electron multiplier” which amplifies the single charge of the ion into a current. The output current of the multiplier (and amplifier) is referenced against the scan voltage, thereby producing a spectrum of peaks. The spectrum produced shows ion current as a function of the quotient mass/charge in a series of peaks corresponding to different ions. The amplitude represents the quantity of each type of ion. Discrete peaks occur because the charged substances have discrete masses and discrete charges (usually single). Generally the terms mass spectrum refers to a spectrum produced by positive ions.

2.5 Kinetic energy distributions

As was mentioned before, the nitroaromatic compounds are able to interact strongly with UV-Vis radiation leading a number of different possible photochemical processes. Has been confirmed laser irradiation of solid energetic materials with ultraviolet (UV) light results in the generation of gaseous molecules or fragments. When those fragments are ejected from the sample they move with a broad range of speeds. Slow molecules are typically formed in thermal processes initiated by laser irradiation, while photochemical processes produce molecules or fragments that have relatively large speeds.

2.5.1 The Maxwell and Boltzmann distributions

At a given temperature, a number of molecules have available energy levels. The continuous agitation that the molecules experience ensures that they are distributed over all available

energy levels. The Boltzmann distribution, gives the formula for calculating the population of states. This formula gives the ratio of the numbers of particles in states with energies E_1 and E_2 as equation 2.1.

$$\frac{N_2}{N_1} = \exp \frac{-(E_2 - E_1)}{kT} \quad 2.1.$$

Where k is the Boltzmann's constant, $k = 1.38 \times 10^{-23} \text{ JK}^{-1}$. It can be observed then, that the distribution is temperature dependent (see figure 8).

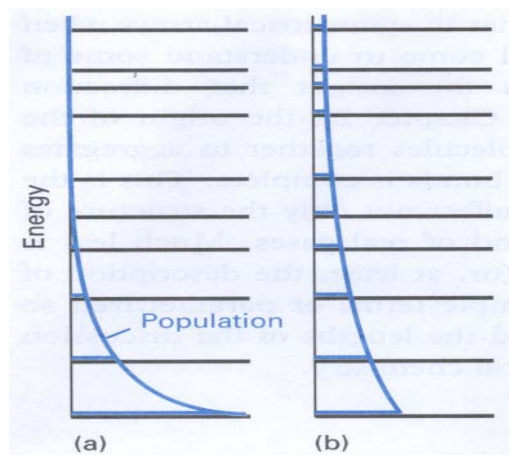


Figure 8. The Boltzmann distribution and population of stated (a) at low temperature. (b) at high temperature.¹³

The Boltzmann distribution predicts that the population of a state decreases exponentially with the energy of the state. At low temperatures, only the lowest states are significantly populated; at high temperatures, there is significant population in high-energy states as well as in low-energy states. At infinite temperature, all the states are equally populated.

The Boltzmann distribution, takes a special form when free translational motion of non-interacting gas molecules are considered. Different energies now correspond to different speeds, so the Boltzmann formula can be used to predict the proportion of molecules having a specific speed at a particular temperature. The distribution of speeds is called the Maxwell distribution and is summarized by the two diagrams shown in figure 9.

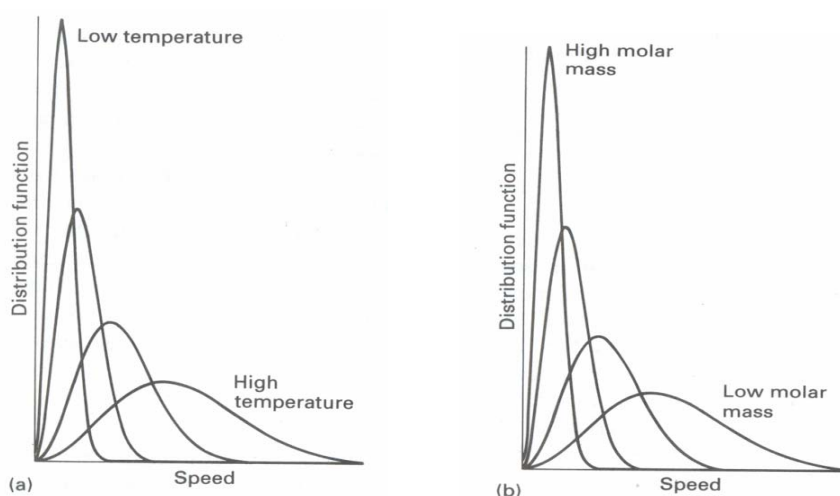


Figure 9. The Maxwell distributions of molecular speeds. (a), The distribution of speeds for a given species of molecule at different temperatures; and in part (b), the distribution of speeds for molecules with different masses at the same temperature.¹³

The Boltzmann and Maxwell concepts as described in the previous paragraphs are widely used to describe energy distribution in systems that are in equilibrium. The results presented in this thesis can not be described by the laws mentioned above due to the non equilibrium nature of the processes. Rather, the study of energy accommodation in photoproducts and molecules are described by molecular dynamics. Several concepts, with different equations,

are borrowed from the classical equations. These include kinetic energy distribution and most probable speed, among others.

2.5.2 Molecular speeds

Because there are such large numbers of gas molecules in any system we are interested in average quantities. Hence, sometimes, the molecular speeds are referred as one representative value, rather, as a whole distribution of speeds. Those representative values are: the most probable speed v_p , the average speed v_{av} , and the root mean-square speed v_{rms} . Figure 10 shows a schematic representation of these values and their respective equations are displayed by equations 2.2., 2.3., and 2.4.

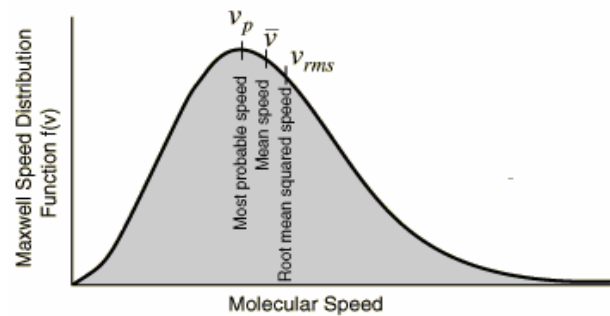


Figure 10. The speed distribution for the molecules given by Maxwell velocity distribution.(obtained from hyperphysics.phy-astr.gsu.edu/.../kintem.html¹⁴, accessed 03/03/06).

$$v_p = \sqrt{\frac{2RT}{M}}$$

2.2.

$$\bar{v} = \sqrt{\frac{8RT}{\pi M}} \quad 2.3.$$

$$v_{rms} = \sqrt{\frac{3RT}{M}} \quad 2.4.$$

The most probable speed is at the maximum of the distribution curve (2.2 equation); the mean speed is slightly to the right of the most probable speed: it has a slightly greater value (2.3. equation), and the root mean squared speed (2.4. equation).

3. EXPERIMENTAL SECTION

The different experimental methods employed to study the photochemistry of TNT, are described in this chapter. Also, a complete description of the experimental set up employed to combine a commercial femtosecond laser and a quadrupole mass spectrometry will be given. A work schedule is presented in figure 11.

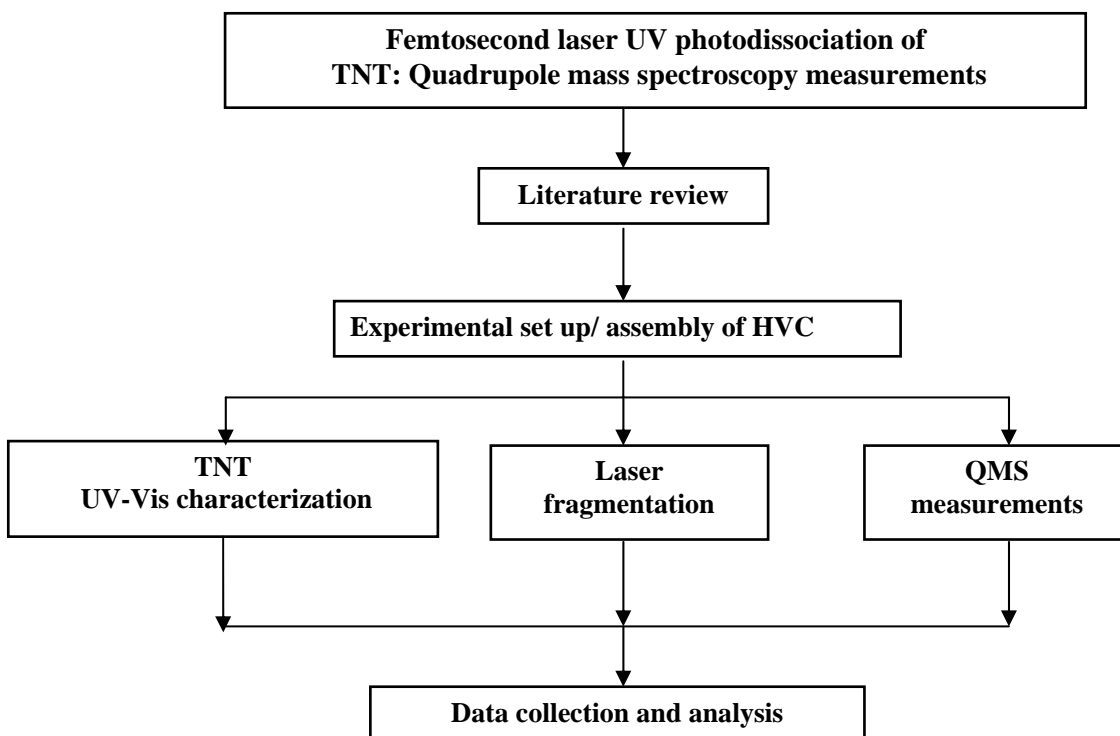


Figure 11. Schematic representation of the experiments conducted to study the laser UV photodissociation of TNT and the quadrupole mass spectroscopy measurements. Samples were constituted by pure solid and gaseous NO_2 .

3.1 Description of the Experimental set-up

Figure 12 presents a scheme of the complete set up used in this work. The experiments were performed in a stainless steel high vacuum chamber (HVC) pumped to pressure of $\sim 10^{-8}$ Torr; the HVC, is equipped for laser spectroscopy and time-of-flight mass spectrometry, the schematic design of the apparatus is shown in figure 12. The apparatus consists of two chambers, the main chamber and an auxiliary chamber. The first consists of an 8-in tee with two ultraviolet (UV) and visible quartz windows, located 90° of each other for laser excitation and /or fluorescence experiments. This chamber is pumped out through the right of the tee by a 700 L/s turbo molecular pump (Varian, Turbo Vacuum 70); on the top of this chamber is mounted a commercial mass spectrometer (Uthe Technology International, UTI-100C precision mass analyzer) . This mass spectrometer is able to distinguish ions of different mass-to-charge ratio. The ionization signals from the QMS, are sent to a computer installed with a Multi-channel Scaler MCS-plus card (EG & Ortec, MCS-plus) for timing applications and TOF data acquisition.

The powder samples of TNT 99% purity, but with a 30% water content, obtained from Chem. Service, were dried under low vacuum at 40°C . Then, these samples were deposited onto the holder located on the end of a rotary-manipulator which is mechanically pumped through a transfer arm. This rotary-manipulator, helps to introduce the sample that will be examined into the main chamber. The laser light from a *Hurricane* Ti:Sapphire laser (Spectra-Physics Lasers) was focused on the sample manipulator containing the sample. The sample was

positioned to face the QMS. The angle between the QMS, sample and incident laser beam is about 45°.

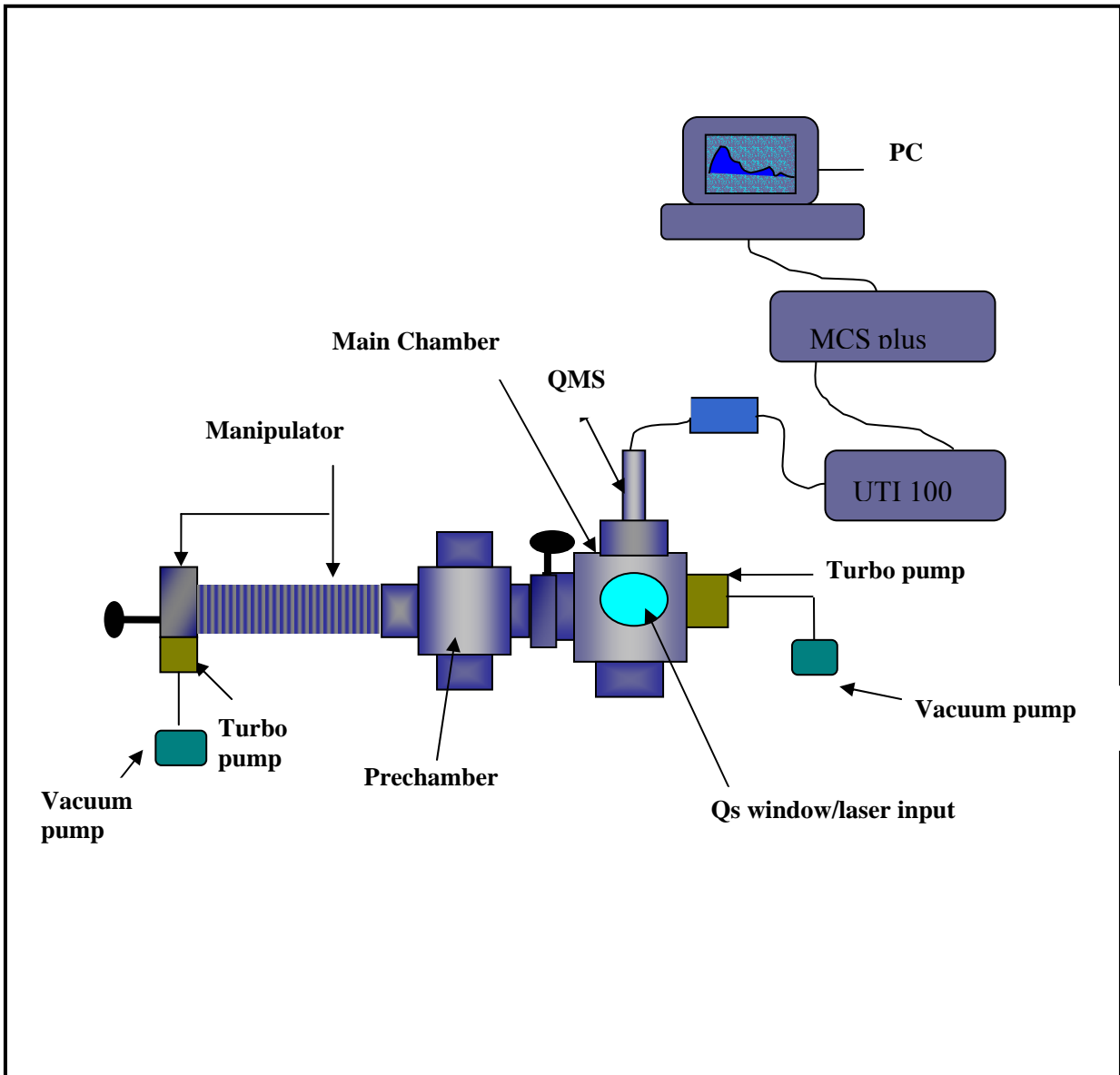


Figure12. Schematic design of Stainless steel high Vacuum Chamber

The source of radiation, consist of a two-laser system, and a continuous wave diode-pumped laser pumps a mode-locked Ti:Sapphire laser that generates pulses of 800 mW. The pulses are taken to a regenerative amplifier, in which the pulses are stretched and amplified while interacting with a Nd:YLF laser. After amplified, the pulses are compressed again to generate even shorter pulses of 100 fs of duration, with energy of approximately 1 mJ. The fundamental radiation is then frequency doubled with the use of a type I phase match crystal to generate 400 nm pulses or frequency tripled by a type I BBO crystal (THG) to generate 266.7 nm pulses. In both cases, the output beam was directed to the fragmentation sampling holder by an optical system, which is constituted by a set of mirrors, UV filters, and a convex lens to focus the laser beam perpendicular to the molecular beam and the mass spectrometer. The fragments released during the photoinduced process were mass resolved in the quadrupole mass spectrometer-QMS- that is located 9.525 cm from the sample holder.

The time of arrival of signals corresponding to NO^+ ($m/e = 30$) and NO_2^+ ($m/e = 46$ amu) was recorded using a MCS-plus card (EG&Ortec) single channel analyzer. Consequently the kinetic energy of the fragments is obtained by dividing the distance from the target to the mass spectrometer by the measured time of arrival provided by the single channel analyzer.

3.1.1. Laser fragmentation

All experiments were performed in synchronization with the arrival of the laser pulses, using a repetition rate of 500Hz. The arrival time began to be registered at the moment the beam stroke the sample and went on until the arrival of another pulse, that is during 2 ms (= 1/500

Hz).. The ultrashort pulses provide a way of creating much higher energy densities in condensed matter, besides, the short pulse duration maximize the peak power of laser and minimize thermal conduction to the surrounding work material due the low repetition rate, permitting that energy that was not used for desorption leave the target zone allowing cooling. Signals for NO₂ and NO fragments were recorded irradiating vapor and solid phases of TNT, during the measurements in solid phase of TNT, the HVC was cooled using a constant flow of liquid nitrogen. For register signal in vapor phase, was used vapor from sublimation of TNT.

3.1.2. Power dependence of signals from fragments

A set of neutral density filters, Melles Griott, were used to perform power dependent experiments. Each neutral density filter has a particular value of optical density at a determined wavelength. From knowledge of the filter's optical density value the power reaching the sample can be estimated.

4. RESULTS AND DISCUSSION

4.1 Mass spectroscopy measurements on TNT

Since a QMS is employed for the measurements described here and TNT has a vapor pressure of the order of 10^{-6} torr we briefly present here a brief discussion on the mass spectrum of TNT. In the UHV chamber employed for the measurements described here, the base pressure is of the order of 10^{-8} torr. Thus upon introduction of solid TNT to the chamber, the base pressure increased to about 10^{-6} Torr due to sublimation of TNT and is large enough to allow us to record the mass spectrum of gas phase TNT. The fragmentation pattern of TNT is displayed in figure 13.

Mass spectroscopy measurements on gas phase TNT revealed a mass spectrum similar in structure to the one measured during irradiation, which is discussed in further detail below. Figures 14 and 15, show the mass spectra for TNT, either at a wavelength at the violet end of the visible spectrum - 400 nm - or one in the UV region - 266 nm - that were employed for these measurements. Both figures show two different scales for specific region of the spectra. The region between 20 and 60 mass/z is reported in a scale of 10^{-4} Amperes (Y axis), and between 60 and 240 mass/z is reported in a scale of 10^{-6} Amperes.

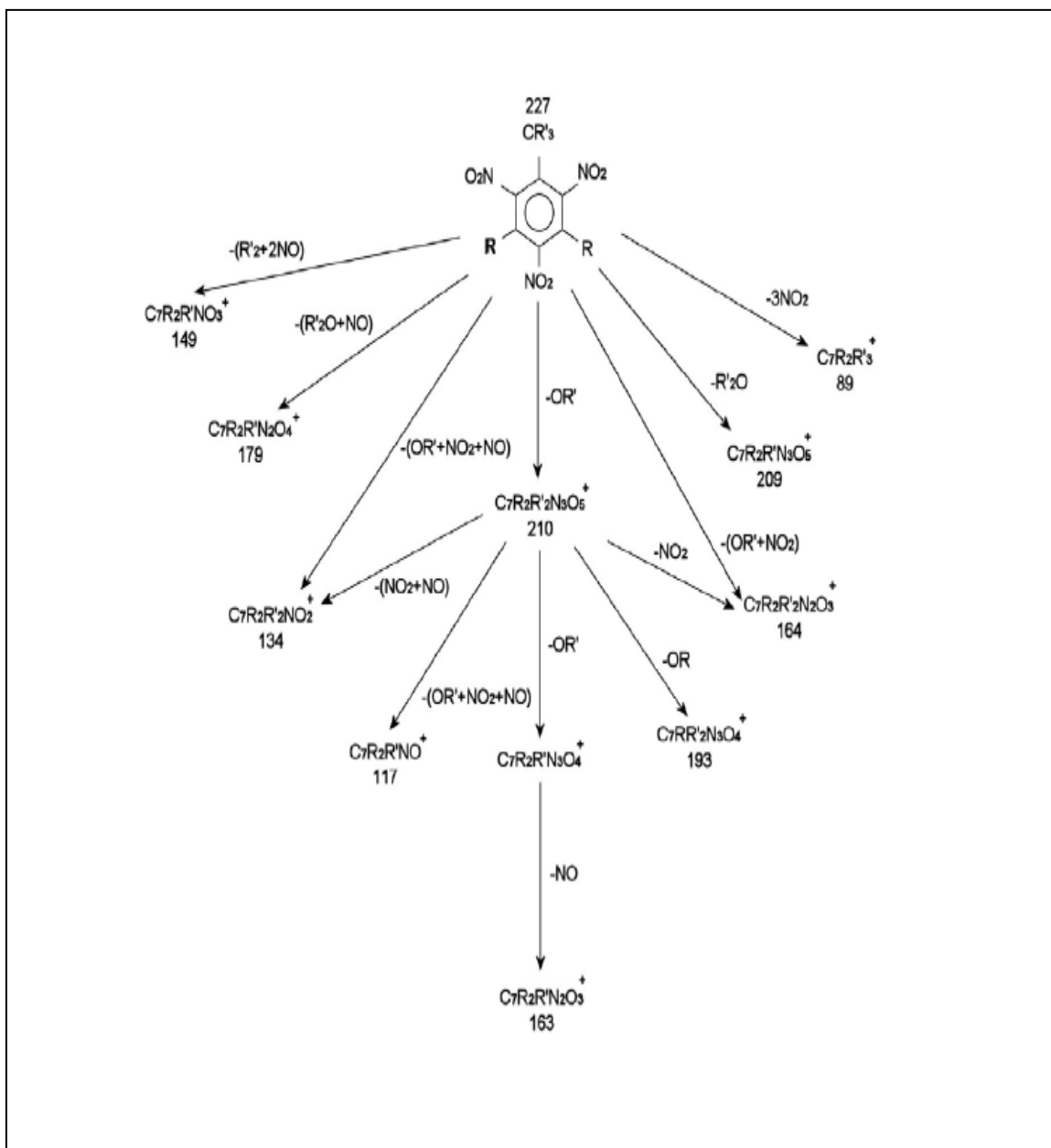


Figure 13. Fragmentation pattern of TNT for positive ions. $R'=H$ from methyl group, $R=H$ from ring¹⁵.

Figure 14, from a to c, shows the Q-MS spectrum of laser photofragmentated 2,4,6-trinitrotoluene (TNT) using 400nm. And figure 16, from a to c, show the Q-MS spectrum of laser photofragmentated 2,4,6- trinitrotoluene (TNT) using 266 nm. The fragmentation pattern is similar at both wavelengths as well as in the absence of any irradiation. The mass spectra of 2,4,6-trinitrotoluene (TNT) recorded using 400 nm or 266 nm wavelength for photofragmentation of parent molecule, exhibit a slight grade of molecular fragmentation yielding to specific and non- specific fragments. In figure 14 a, the mass spectrum shows ion signals characteristic for TNT: $[\text{C}_6\text{H}_2\text{CH}_2\text{N}_3\text{O}_5]^+$ (210 m/z), $[\text{C}_6\text{HCH}_2\text{N}_3\text{O}_4]^+$ (193 m/z), $[\text{C}_6\text{H}_2\text{CHN}_2\text{O}_4]^+$ (179 m/z), $[\text{C}_6\text{H}_2\text{CHN}_2\text{O}_3]^+$ or $[\text{C}_6\text{H}_2\text{CHN}_3\text{O}_5]^+$ (163 or 164 m/z), $[\text{C}_6\text{H}_2\text{CHNO}_3]^+$ (149 m/z), and $[\text{C}_6\text{H}_2\text{CH}_2\text{NO}_2]^+$ (134 m/z) according to the most probable fragmentation channels proposed by Yinon¹⁵ as is shown in figure 13. These dissociative channels arise from the loss of H, O, NO and NO₂ from the TNT molecule. Additionally, the mass spectra either figure 14b and figure 14c, show the characteristic fragments $[\text{NO}_2]^+$ (46 m/z) and $[\text{NO}]^+$ (30 m/z) from nitro groups of the parent molecule. Also, both mass spectra in figure 14a, and 15a, lack the molecular ion peak despite the mild fragmentation of the molecule, upon ultrashort UV laser pulses. That is due the low energy needed for dissociation of nitro groups, and the fact that they provide a number of dissociation paths. Actually, a common feature of nitro compounds is their low barrier for dissociation and the fact that they provide a number of dissociation pathways. Other studies have also demonstrated that nitrotoluenes are ionized either by four or a two photon process, and when the radiation of ultrashort UV laser pulses are employed the degree of fragmentation during the multiphoton ionization process is reduced.¹⁶

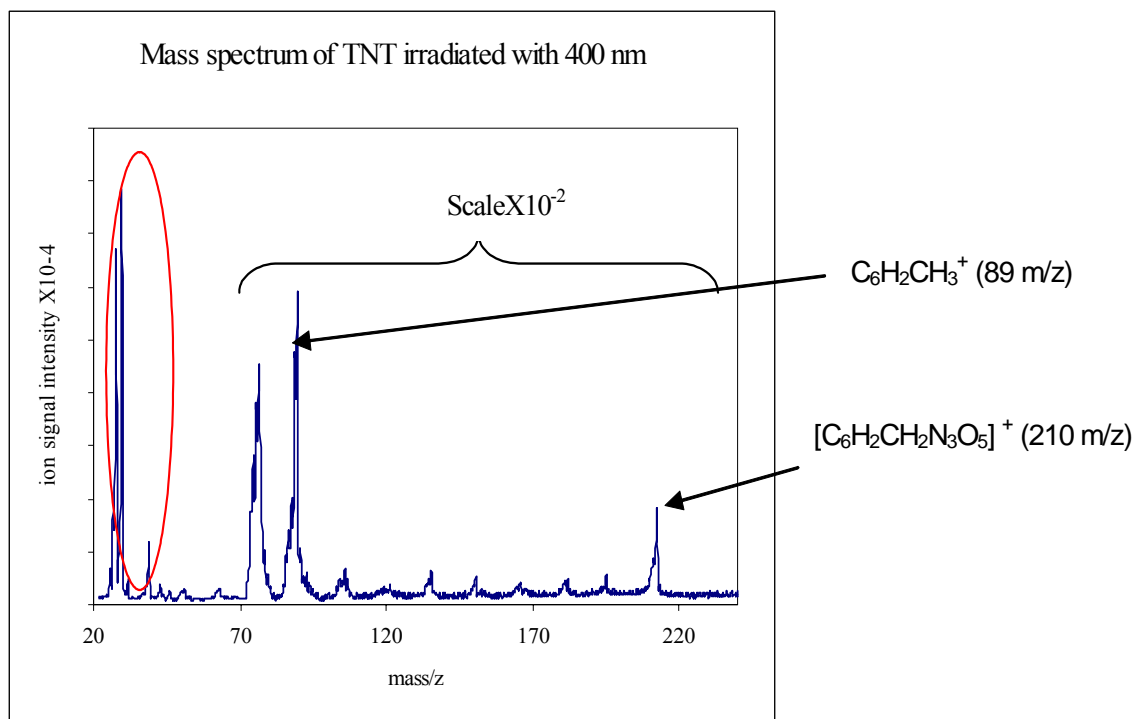


Figure 14a. *Q-MS* spectrum of laser photofragmentated 2,4,6- trinitrotoluene (TNT) using 400 nm.

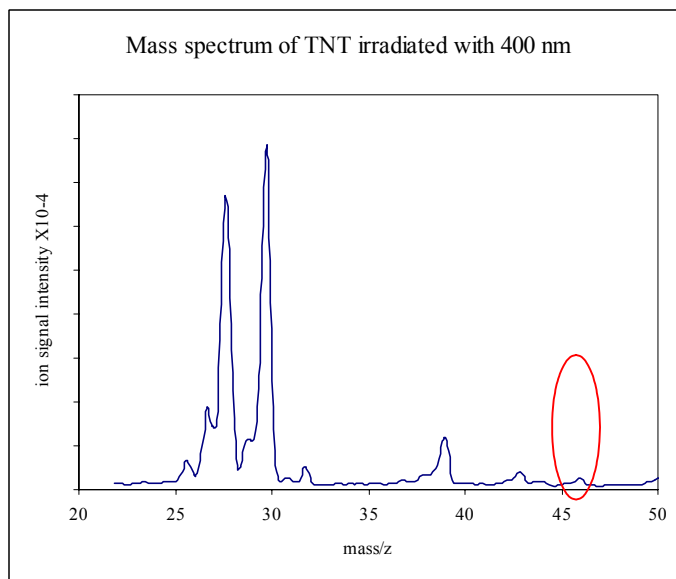


Figure 14b. Detail of *Q-MS* spectrum of laser photofragmentated 2,4,6- trinitrotoluene (TNT) using 400 nm showed in figure 14a .

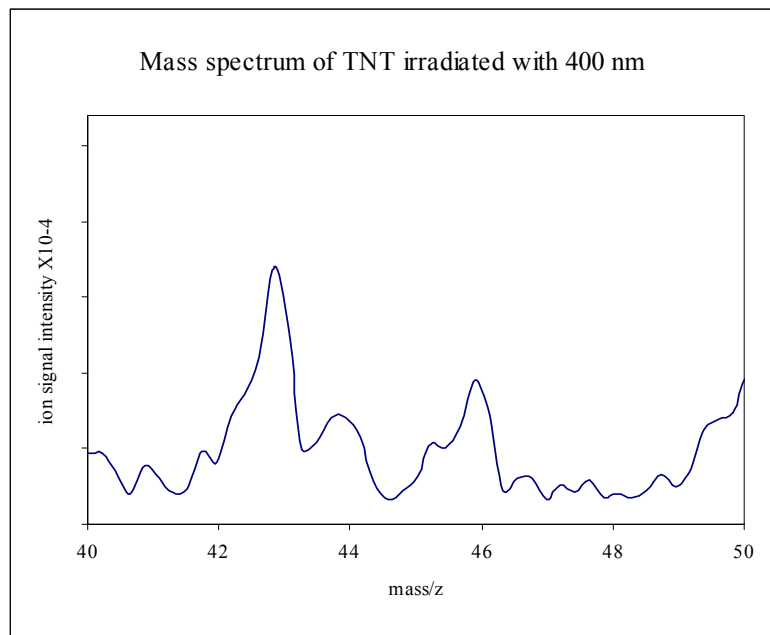


Figure 14c. *Q-MS spectrum of laser photofragmented 2,4,6- trinitrotoluene (TNT) using 400 nm showed in figure 14b.*

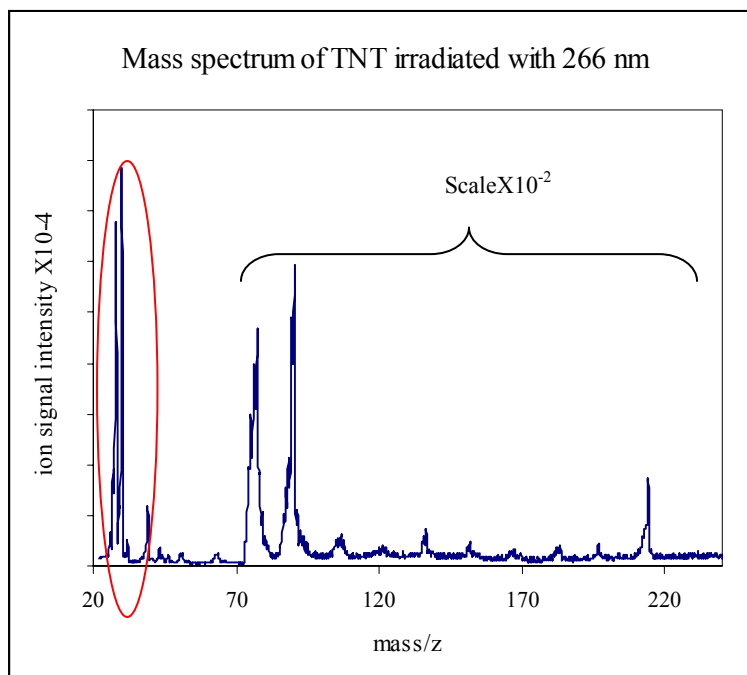


Figure 15a. *Q-MS spectrum of laser photofragmented 2,4,6- trinitrotoluene (TNT) using 266 nm .*

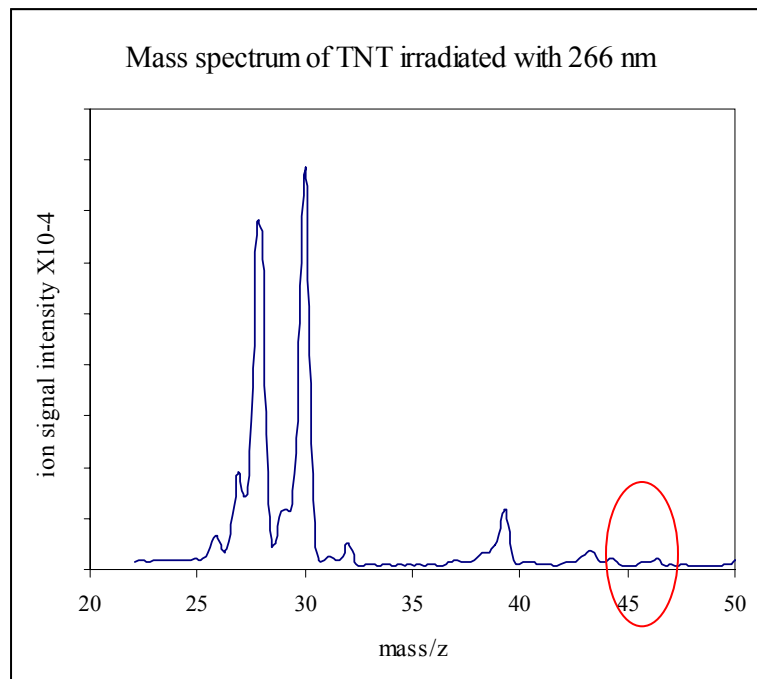


Figure 15b. Detail of the Q-MS spectrum of laser photofragmentated 2,4,6-trinitrotoluene (TNT) using 266 nm showed in figure 15a..

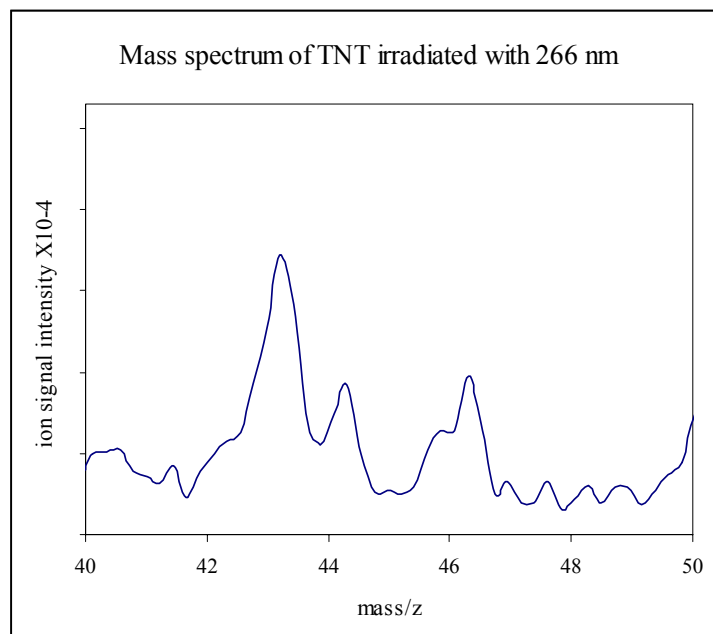


Figure 15c. Detail of Q-MS spectrum of laser photofragmentated 2,4,6- trinitrotoluene (TNT) using 266 nm showed in figure 15b .

4.2 Light absorption by solid TNT

Figure 16 shows the absorption spectrum of TNT. The optical absorption spectrum of TNT was obtained from independent measurements, using a high-pressure deuterium arc lamp and a multidiode array photodetector. For the measurements, TNT powder was deposited on an aluminum foil substrate. The light from the lamp strikes the sample at an angle of 45° and the reflected light is collected by a UV grade optical fiber at an angle of 45° and fed into the spectrograph.

The spectrum reveals a broad absorption band between 250 and 500 nm with a high wavelength shoulder at about 450 nm. Also, the spectroscopic fingerprint of TNT between 395 and 495 nm was determined from transmission near field optical microscopy measurements.¹⁷ Light absorption into the visible region of the spectrum can not be attributed to the π to π^* transitions in the aromatic ring. In benzene, these transitions are observed well below 300 nm. The transitions observed here must result from excitation of electrons associated with the nitro group and may involve $n \rightarrow \pi^*$ and $\pi \rightarrow \pi^*$ transitions localized in the $-\text{NO}_2$ group or from non bonding electrons in the NO_2 group into the aromatic π^* system of the molecule. For NO_2 , the dissociation threshold is around 398 nm¹⁸, close to the maximum absorption wavelength of free NO_2 . The two wavelengths employed in the time-of-flight measurements allow us to interrogate the photochemistry of TNT in the UV-visible region of the spectrum.

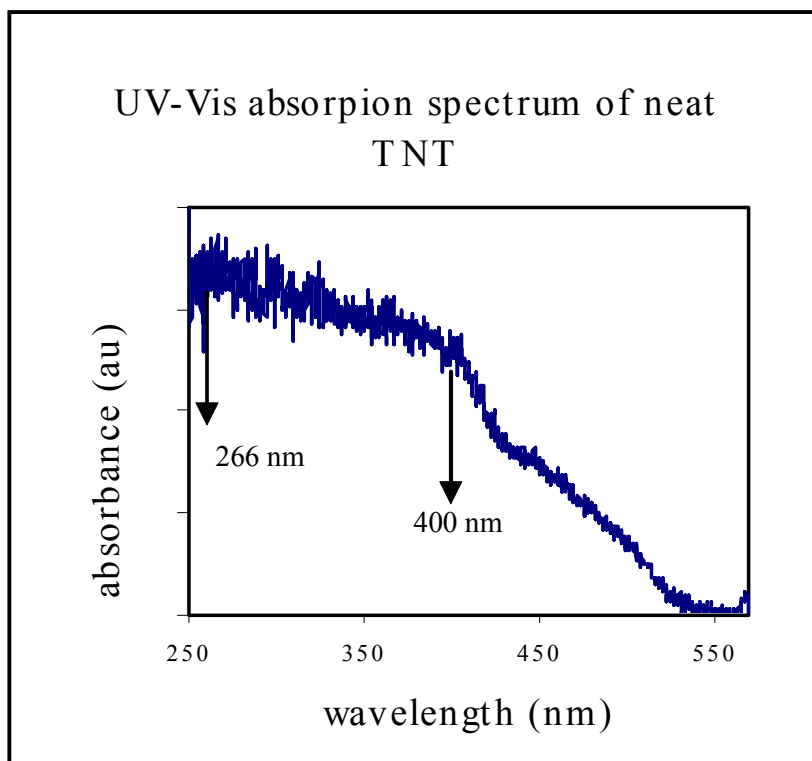


Figure 16. UV-Vis absorption spectrum of neat TNT

4.3 Time-of-Flight measurements

The dynamics of the target fragments NO_2 and NO released during photo-fragmentation were studied using time-of-flight measurements. The experiments were performed in synchronization with the arrival of the laser pulses and a repetition rate of 500Hz (= 2 ms). The time profile of the laser shots from the Hurricane system is illustrated in Figure 17. The wavelength is 266 nm and the repetition rate is 500 Hz. For the measurements, a UV sensitive photo detector was placed in front of the 266 nm light. The photo detector output is fed into the MCS plus data acquisition. For the TOF measurements described here, data collection begins at time $t=0$ seconds, upon the arrival of the laser pulse to the target surface and continues until the arrival of the second laser shot, which restarts the cycle. The data

displayed on figure 17 illustrates the stability of the laser intensity and repetition rate as monitored by the UV sensitive photo detector and the reliability of the Hurricane repetition rate settings.

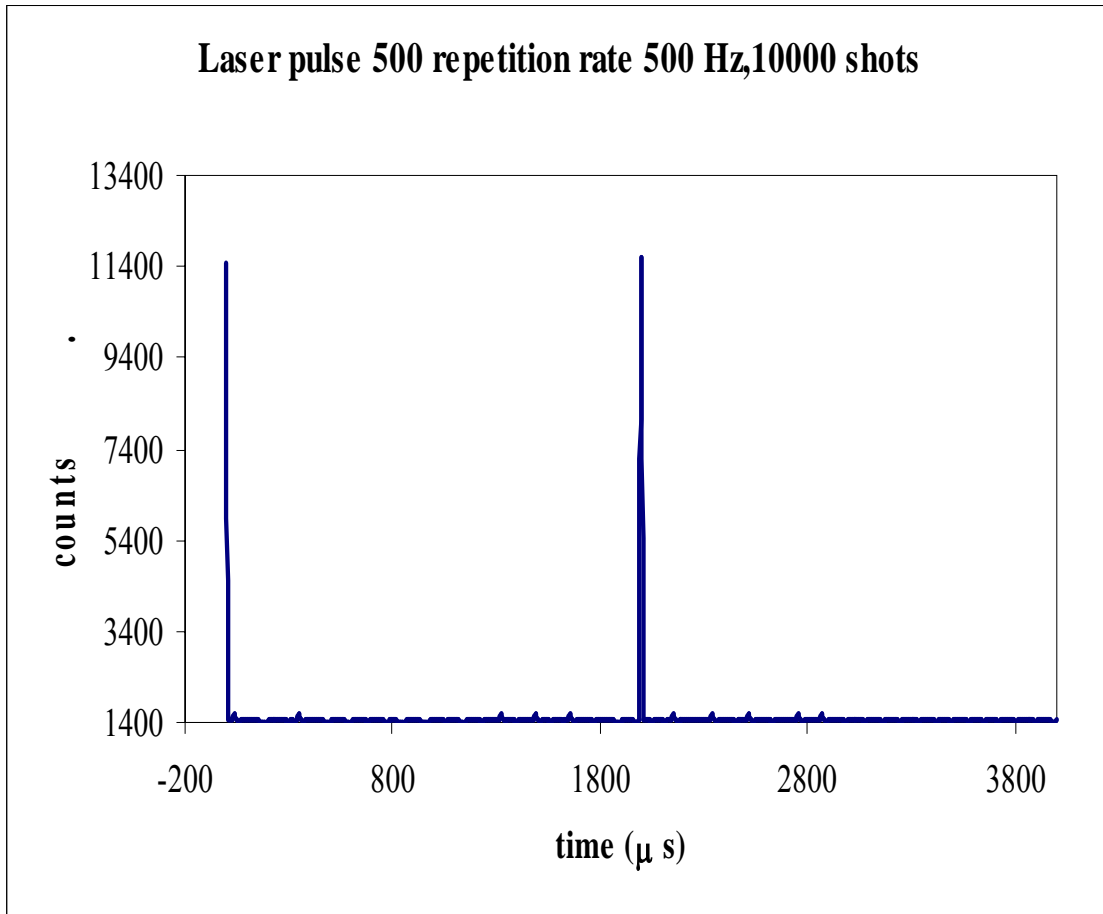


Figure 17. Pulses of Hurricane Ti:Sapphire laser (Spectra-Physics Lasers), recorded with MCS -plus card

4.3.1. Raw data: Arrival curves for NO₂ and NO fragments.

As the laser beam hit the sample the signals from quadrupole mass spectrometer were feed to the MCS single channel analyzer that registered the arrival of signals as a function of time.

Figures from 18 to 21 show the results obtained for 266 nm and 400 nm of laser irradiation. Those results presented here are representative result over an average of five runs for experiment, and were taken over 20000 laser shots. The measurements are not corrected for TNT fragmentation or ion transmission through the mass spectrometer.

Figure 18, shows the arrival curves for NO₂ fragment ejected from TNT using 266 nm wavelength irradiation and figure 19, shows the arrival curves for the NO fragment originating of the TNT radiated with 266 nm of wavelength.

In the arrival curves, 18, the maxima intensity signal for the NO₂ fragment occurs at 60 μ s. Also, is possible to observe, that for the fragment of NO₂, the signal intensity is higher when the vapor of the TNT is irradiated than when the crystal is irradiated. Additionally, figure 19, shows the signal intensity for NO fragments as a function of time. In this plot, it can be observed that, the signal increases since the 60 μ s and, is higher when solid TNT is irradiated than when the vapor phase is irradiated.

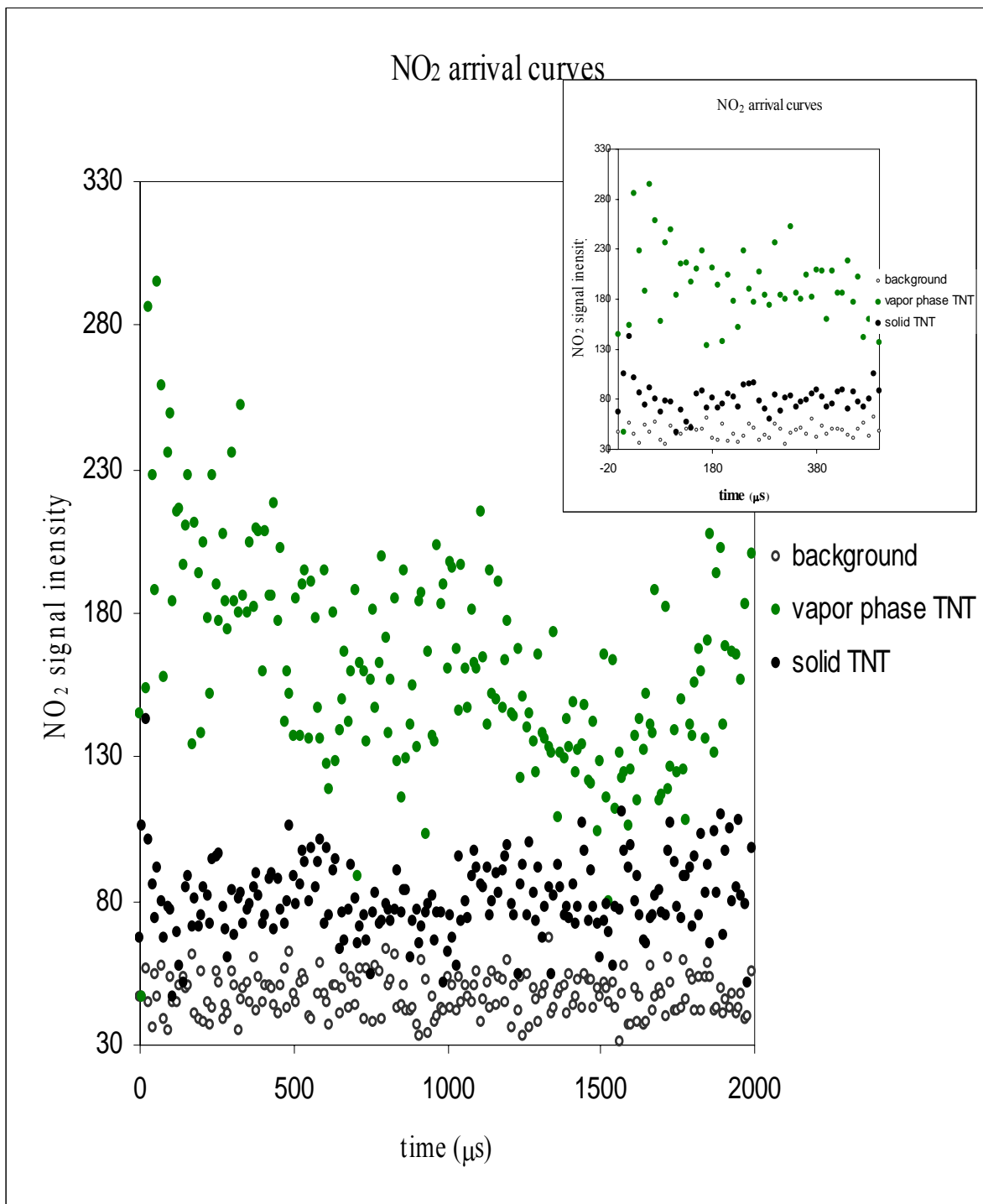


Figure 18. arrival curve for NO₂ fragment ejected from TNT using 266 nm wavelength irradiation.

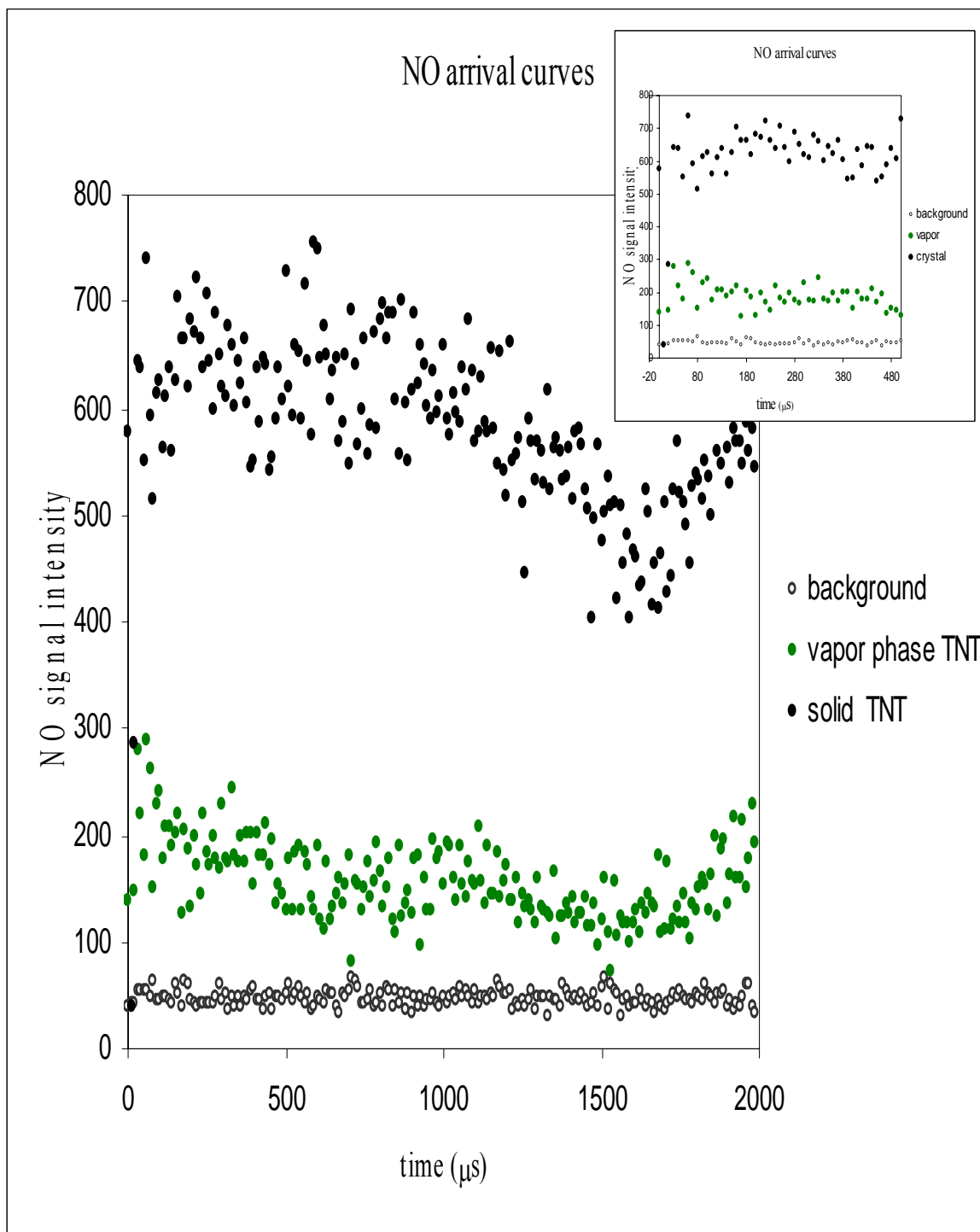


Figure 19. arrival curve for NO fragment ejected from TNT using 266 nm wavelength irradiation.

Figure 20 and figure 21, show the arrival curves for the NO_2 , and, NO fragment evicted from the TNT radiated with 400 nm wavelength, respectively.

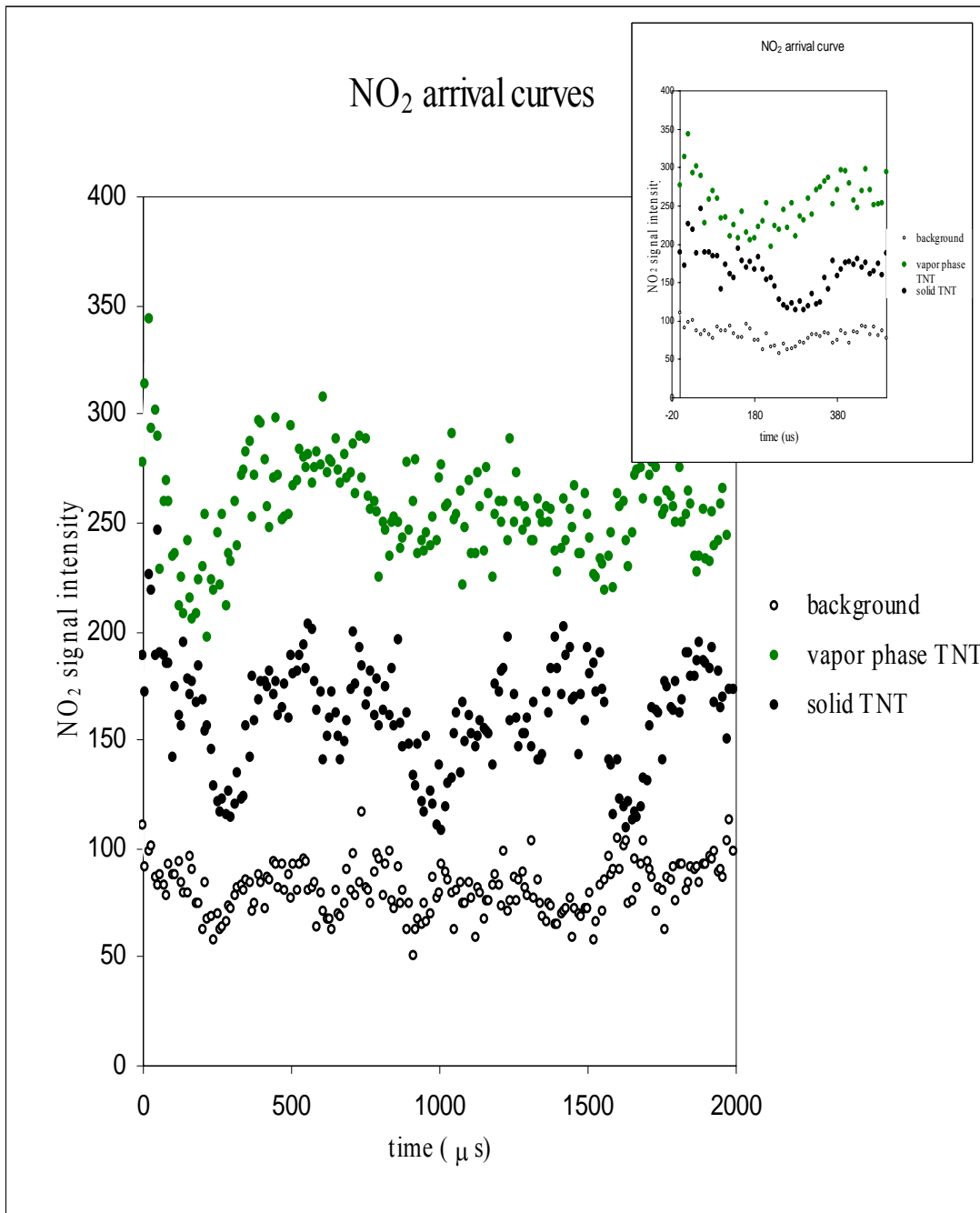


Figure 20. Arrival curves for NO₂ from TNT, 400 nm wavelength

Figure 20, shows the signal intensity for NO_2 fragments as a function of time. This plot, shows that, the maxima signal for the NO_2 fragment, since the $20 \mu\text{s}$ is greater when vapor phase of TNT is irradiated than when solid neat TNT is irradiated. In contrast, the signal for the NO fragment, showed in the figure 21, indicates that the maximum signal for NO fragment arising since $30 \mu\text{s}$. This signal is higher when solid neat TNT is irradiated than when vapor phase TNT is irradiated. This fact indicates that, the NO fragment is produced in the ionization region of the quadrupole mass spectrometer but by photofragmentation due the 400 nm radiation.

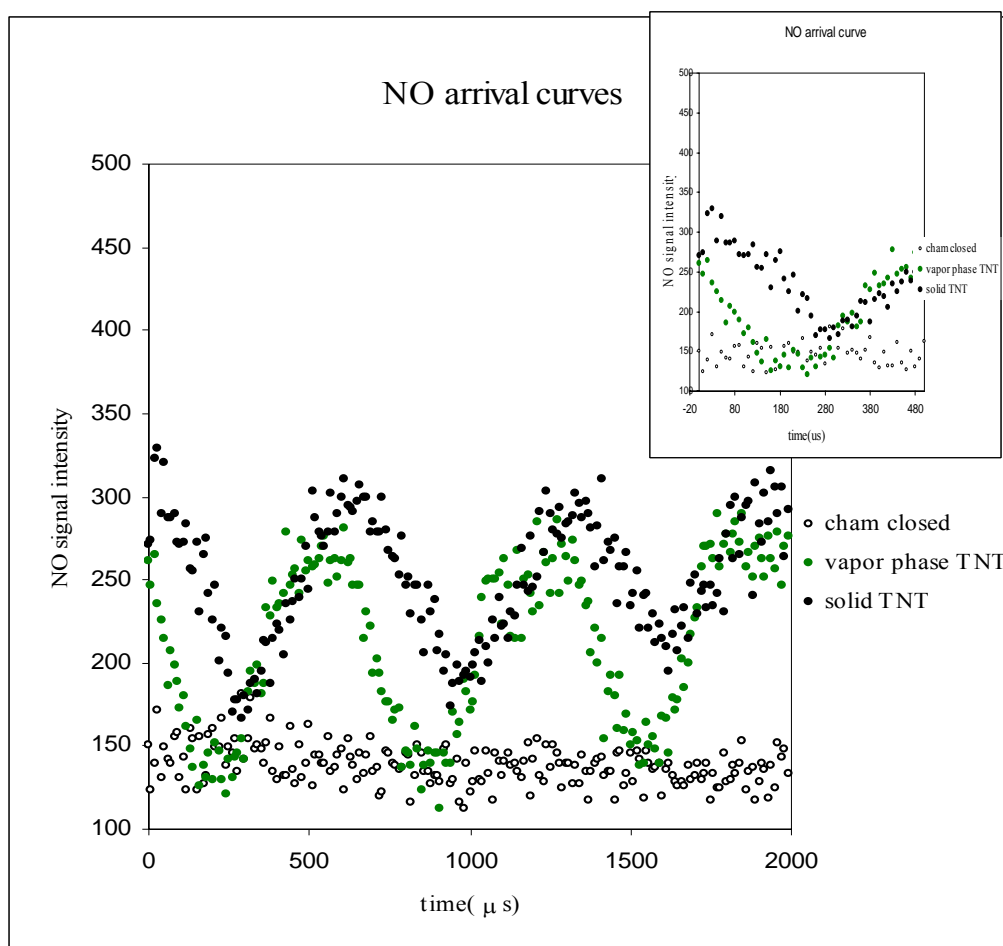


Figure 21. Arrival curves for NO_2 from TNT, 400 nm wavelength

4.3.2. Power dependence of NO₂ and NO signals

The arrival curves for NO₂ and NO fragments were recorded upon de radiation of the pulses of laser varying the power of laser. For each fragment, the highest intensity of each signal was measured and referred against the power of laser.

Figures 22 and 23 show the dependence of the high energy peaks that appear in the NO and NO₂ signal intensities, respectively.

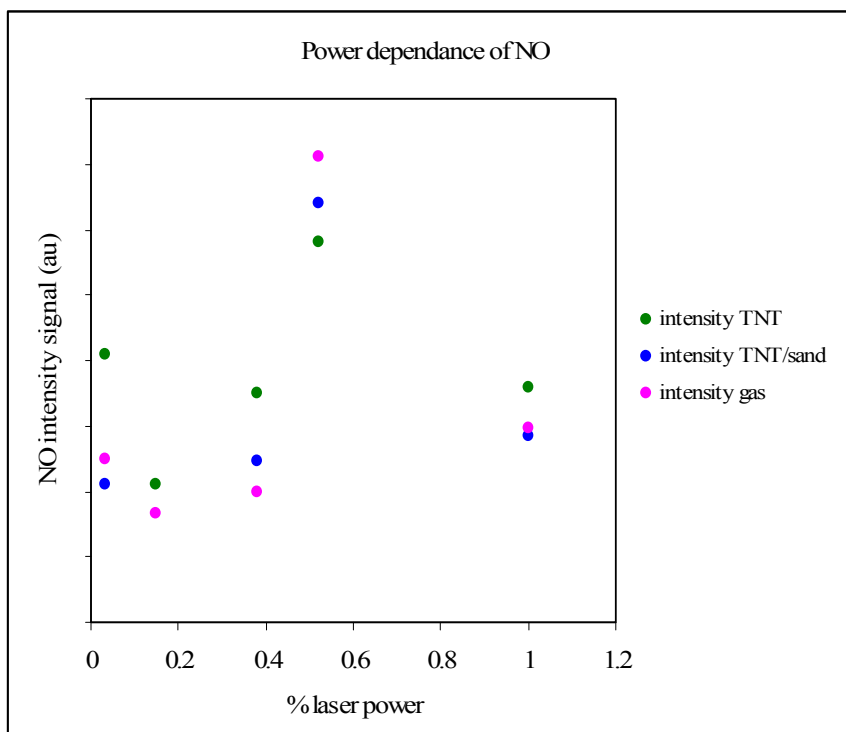
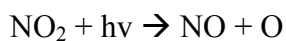
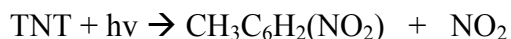


Figure 22. Dependence of high kinetic energy distribution peak intensity of NO on excitation laser power.

Both peak intensities exhibit local maxima. For NO, the maximum is observed at excitation powers that are about 60 % that of the nominal excitation power delivered from the laser.

For NO₂, the maximum occurs at about 20 % of the nominal excitation power delivered from the laser. The observed dependence of the NO and NO₂ kinetic energy distributions is according to the multiphotonic process described by reactions below.



The second step, the photodissociation of NO₂ requires an additional photon, which is readily available upon increasing the laser power.¹⁹ Thus it can be extrapolated that the signal intensity is higher for different power of radiation depending on the type of fragmentation taking place, this is primarily due to the different energy and power needed for the photolysis of each molecule.

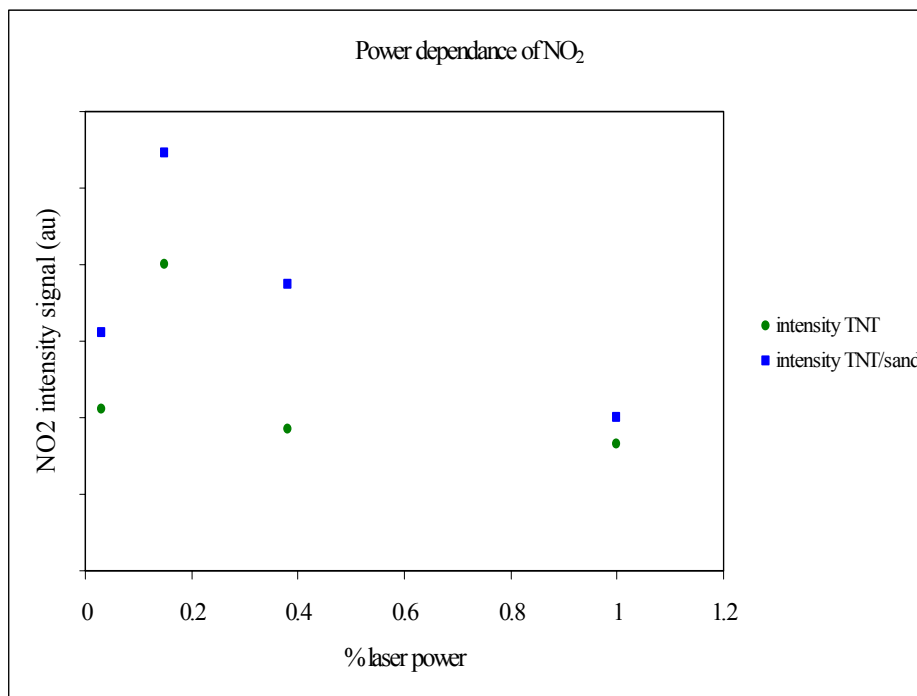


Figure 23. Dependence of high kinetic energy distribution peak intensity of NO₂ on excitation laser power.

4.3.3. *Manipulated data: Distribution of kinetic energy for NO₂ and NO fragments.*

Next figures 24 a and b, and 25 a and b, show the distribution of speeds for the NO₂ fragment from TNT, upon wavelength of 266 nm radiation and the distribution of speeds for the NO fragment originating from the TNT radiated with 266 nm of wavelength.

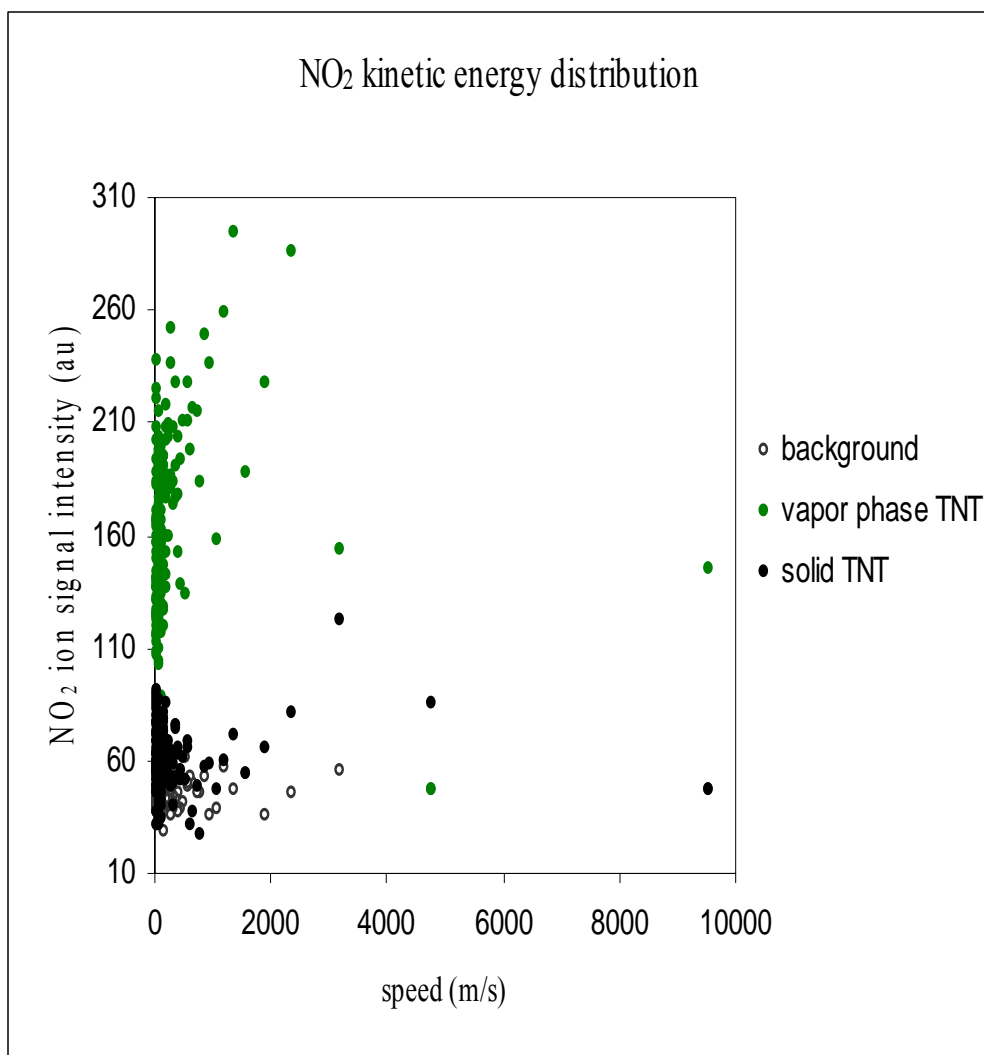


Figure 24a . Kinetic energy distribution of NO₂ from TNT, 266 nm wavelength

Figure 24a, shows a higher signal for the NO₂ fragment when vapor phase of TNT is irradiated than when solid phase is irradiated. Conversely, in figure 25a, the plot for the distribution of speeds, shows that the signal for NO fragment is higher when the solid sample was radiated. The reason could be the result of the process of absorption of two photons by the molecule of TNT, the first for the dissociation of NO₂ and second photon for the dissociation of the later to produce the NO fragment which is according to multiphotonic nature of this process, as illustrated by the reaction below:



The molecule of TNT, absorbs a UV photon with energy equal or greater than 2.6 eV and produces molecular NO₂ fragments. Then NO₂, absorbs another UV photon (with energy equal or greater than 3.11 eV) and produces the NO fragment.

Moreover considering that the energy necessary to dissociate NO₂ in NO, is approximately 3.11 eV, and the wavelength of 266 nm, corresponds to an energy of 4.67 eV, this implies that 1.56 eV, confer to the fragment NO a greater kinetic energy that allows those to cross the distance from the site of the ablation to the mass spectrometer, surviving the collisions with the other fragments that are taking place, and which could interrupt its trajectory until the region of ionization of quadrupole.

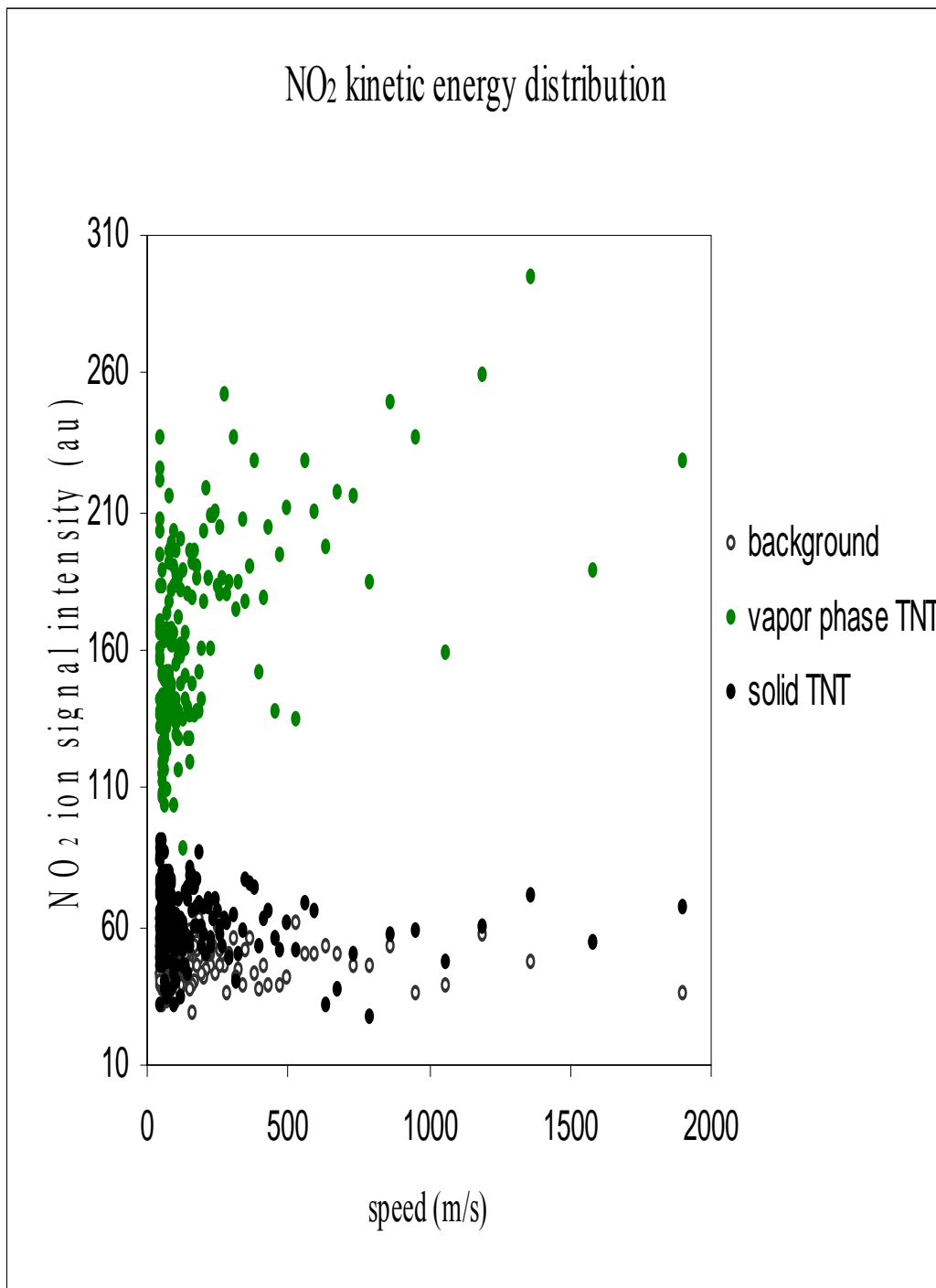


Figure 24b . Kinetic energy distribution of NO₂ (detail of figure 24a, in the region from 0 to 2000 m/s) from TNT, 266 nm wavelength

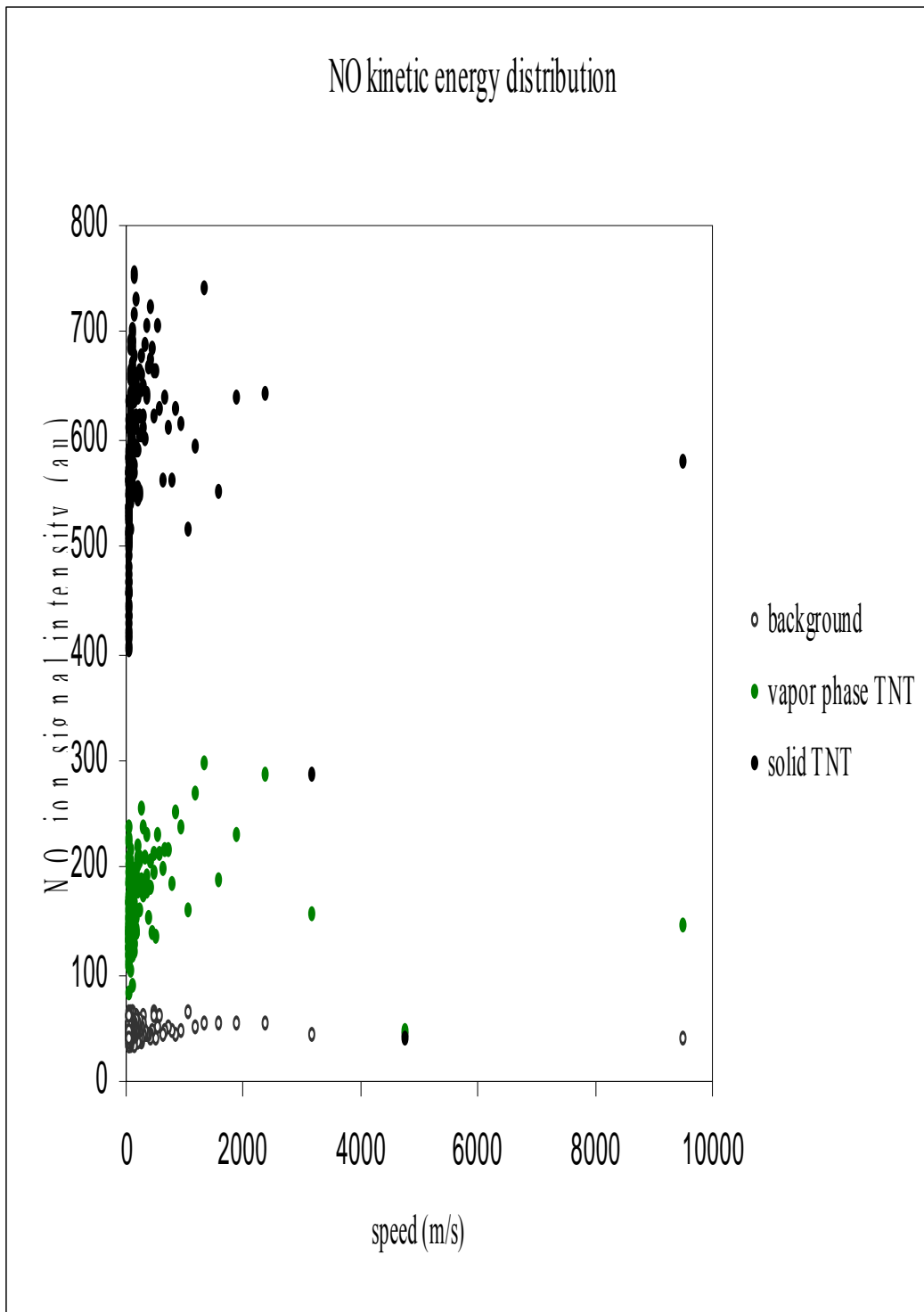


Figure 25a. Kinetic energy distribution of NO from TNT, 266 nm wavelength

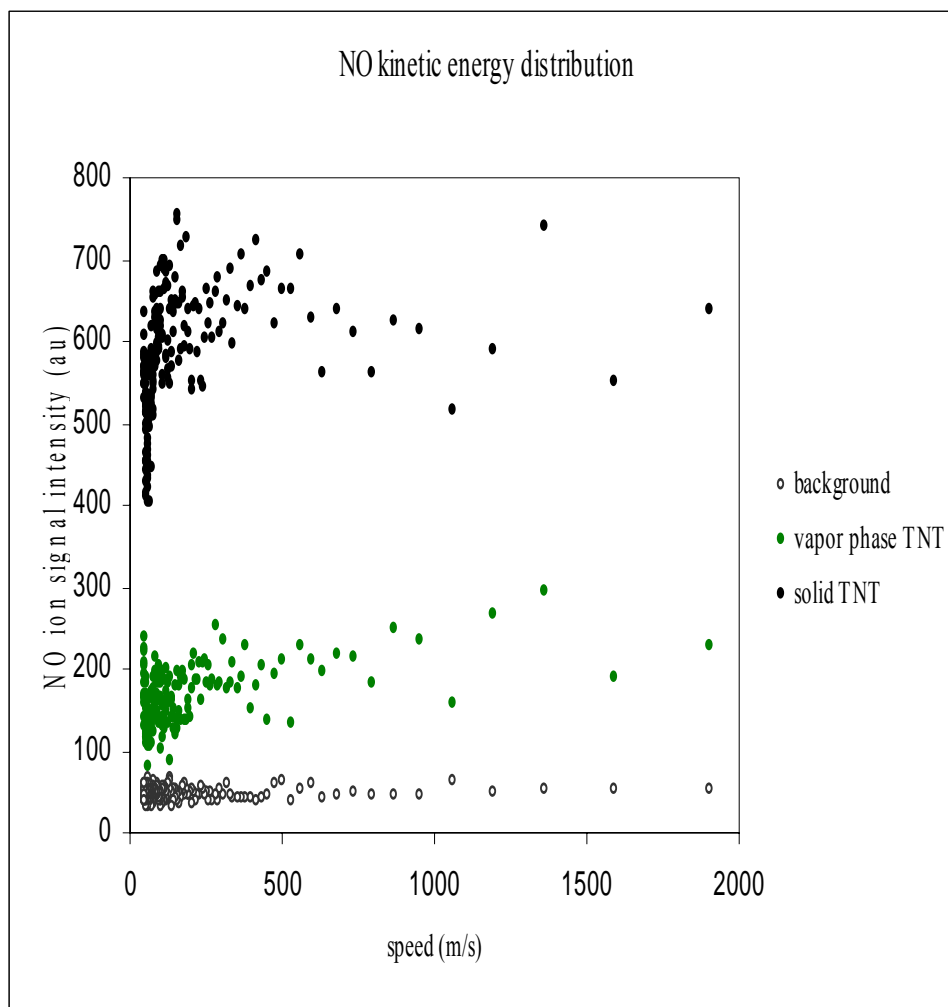


Figure 25b. Kinetic energy distribution of NO (detail of figure 25a, in the region from 0 to 2000 m/s) from TNT, 266 nm wavelength

Alternatively, figure 26, displays distribution of speeds for fragment of $C_6H_2CH_3^+$ (89 m/z) originating from TNT radiated with 266 nm of wavelength, that fragment corresponds to the TNT when its three nitro groups are lost. The higher signal intensity occurs when the solid TNT is radiated, this once again corroborates the raised hypothesis to explain the results shown in figure 25, corresponding to the distribution of speeds for the NO fragment.

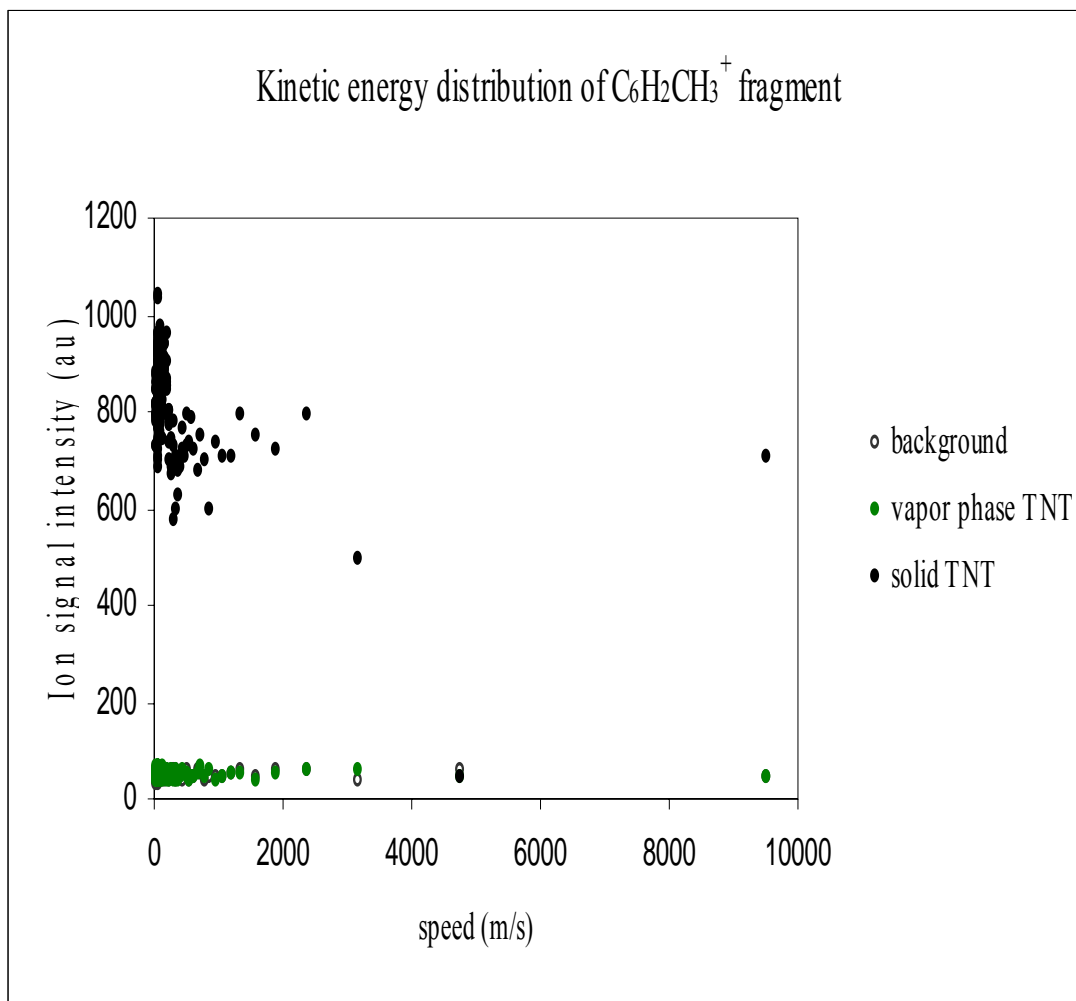


Figure 26. Kinetic energy distribution of 89 m/z fragment from TNT, 266 nm wavelength

Figure 27 a and b, and figure 28 a and b, show the kinetic energy distribution for the NO_2 , and, NO fragment evicted from the TNT radiated with 400 nm wavelength, respectively.

In the NO_2 velocity distribution, figure 27a, different patterns are observed for vapor phase and condensed phase of TNT. Showing a higher intensity of signal for the irradiation of vapor phase of TNT than for irradiation of condensed phase of TNT, which agrees with

observed upon 266 nm. Conversely, with signal behavior for NO in figure 28a. In the velocity distribution for NO fragment plot, is possible observe that the distribution pattern is different for the irradiation of gaseous phase from the distribution pattern for the irradiation of condensed phase, either neat TNT or TNT deposited on sand. This fact is related to the origin of the observed NO fragment upon 400 nm, this wavelength cannot afford the dissociation of NO_2 to produce NO fragment; else, this signal is resulting of the interaction of ejected NO_2 fragment with the quadrupole's ionization region.

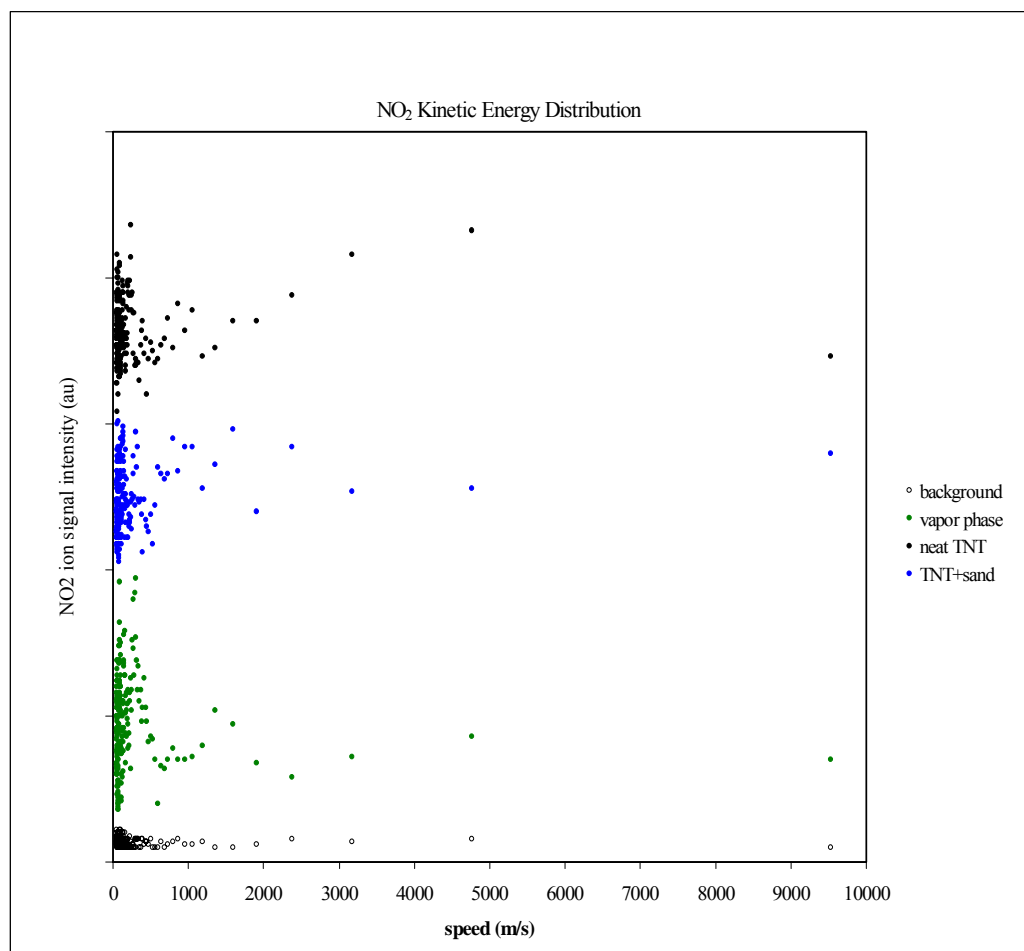


Figure 27a. Kinetic energy distribution of NO_2 from TNT, 400 nm wavelength

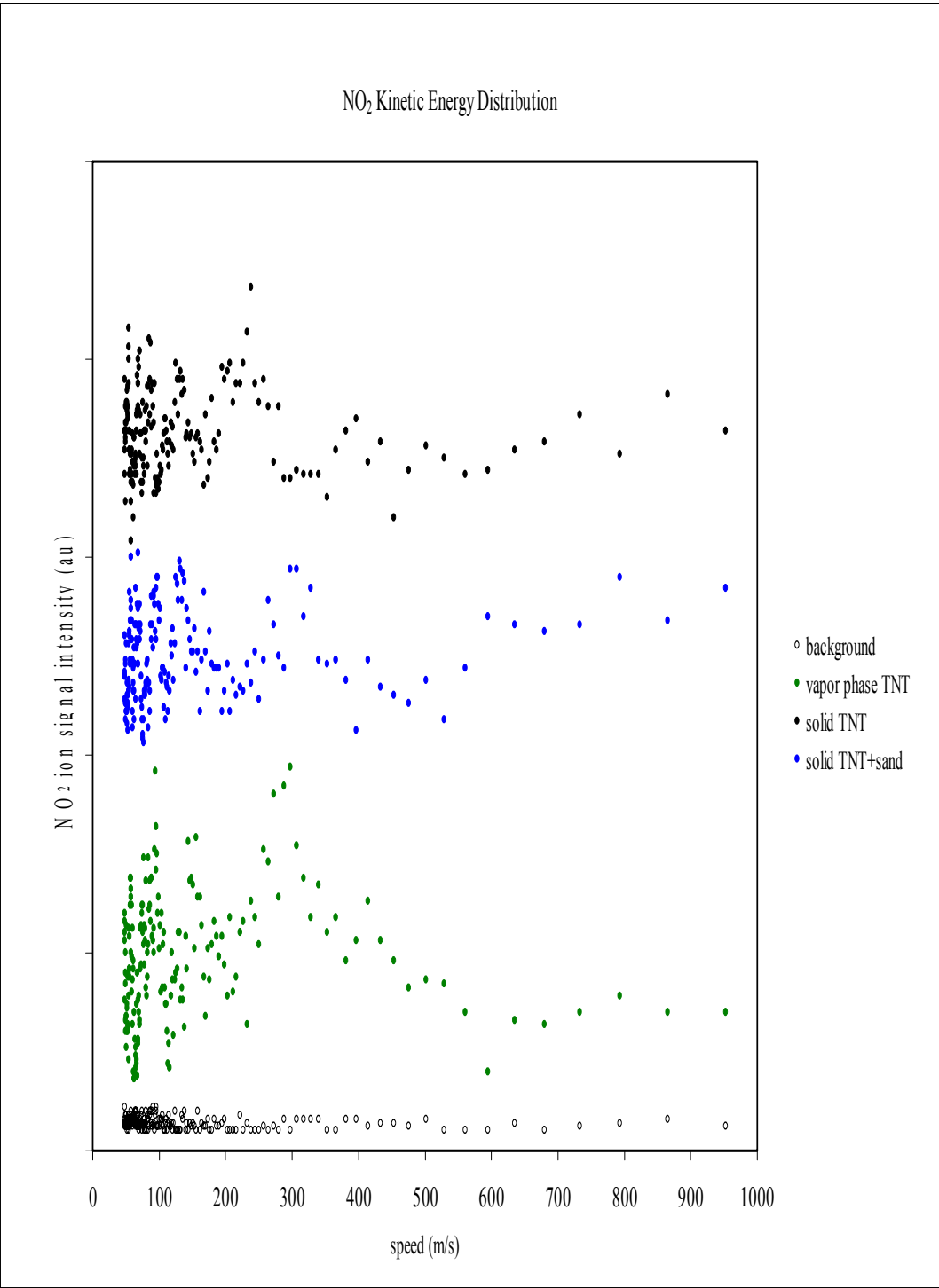


Figure 27b. Kinetic energy distribution of NO₂ (in the region from 0 to 1000 m/s from TNT, 400 nm wavelength

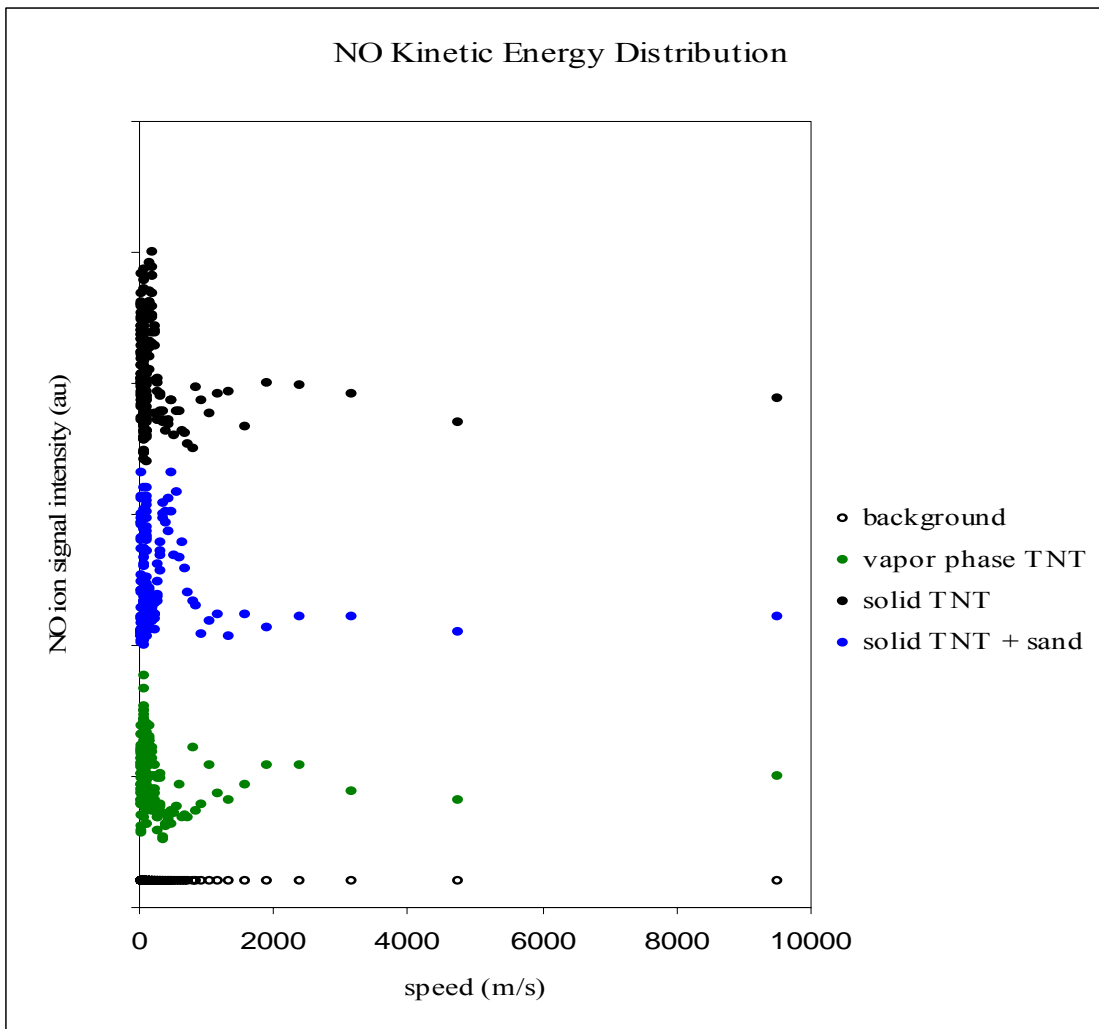


Figure 28a. Kinetic energy distribution of NO from TNT, 400 nm wavelength

In addition, in both cases, figure 27a and figure 28a, the peaks of higher signal are present velocities below the most probable velocity values at room temperature, according with the Maxwell and Boltzmann distribution. That is a proof of the photochemistry nature of the process. Since, upon laser irradiation of solid materials, both, photothermal and

photochemical processes can produce molecular fragments from the irradiated surface⁵, the kinetic energy distribution or velocity distribution helps to discriminate what process is occurring. The data here presented reveals the photochemical character of the fragmentation of TNT molecule using femtosecond laser pulses either with 266 nm and 400 nm wavelength. This fact is primarily due two factors: first, due the photolabile nature of NO₂ group weakly attached to the TNT molecule, and due the use of ultrashort pulses in a low repetition rate. For these reasons, the kinetic energy distribution obtained for NO_x fragments from TNT, do not follow the Maxwell-Boltzmann distribution, which are consistent with photothermal processes^{16,20}.

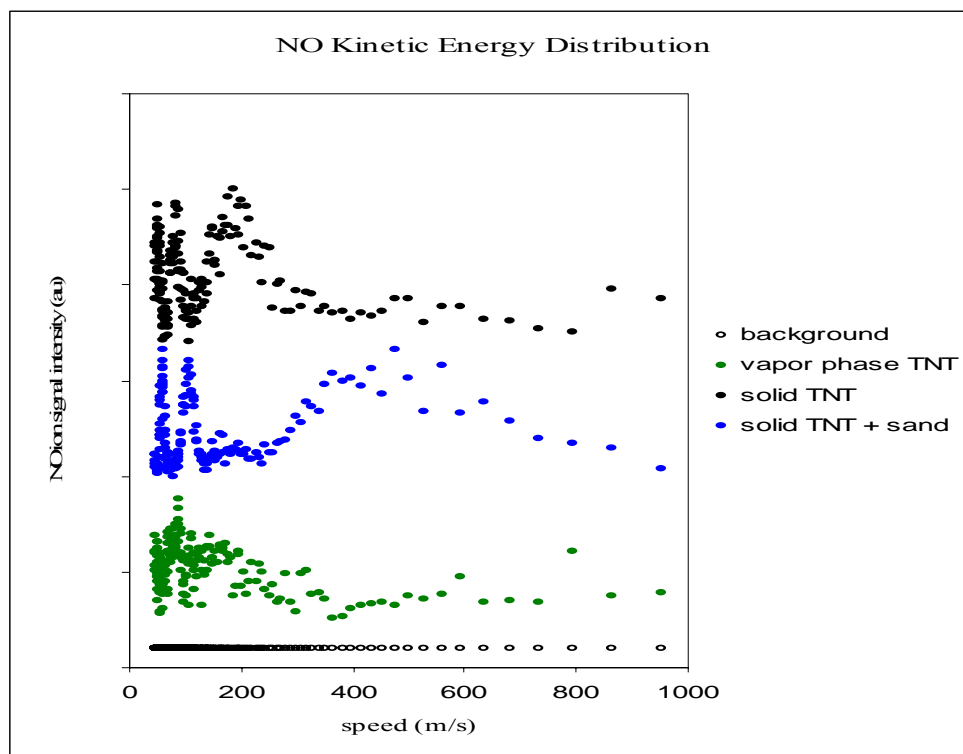


Figure 28b. Kinetic energy distribution of NO (in the region from 0 to 2000 m/s) from TNT, 400 nm wavelength

4.4 Comparison between velocities of fragments and Boltzmann distribution.

The data of the fragments released during the ablation process with the laser radiation, was obtained using the quadrupole mass spectroscopy technique and then coupled to the multichannel scaler card. This system, permitted the recording of the time of arrival of the released fragments, in order to establish the arrival curves and finally by analyzing the data the kinetic energy distribution of the target fragments that is, NO and NO₂ was extracted.

In figures 22 a and b, and 27a and b, the peaks of higher signal are present velocities below the most probable velocity values at room temperature (v_p NO \approx 406 m/s and v_p NO₂ \approx 328 m/s at T= 298 K), according with the Maxwell and Boltzmann distribution for processes in equilibrium. That is a proof of the photochemistry nature of the process (non equilibrium processes). Since, upon laser irradiation of solid materials, both, photothermal and photochemical processes can produce molecular fragments from the irradiated surface^{4,21}, the kinetic energy distribution or velocity distribution, helps to discriminate what process is occurring. The data here presented reveal the photochemical character of the fragmentation of the TNT molecule using femtosecond laser pulses either with 266 nm and 400 nm wavelength. This fact is primarily due two factors: first, due the photolabile nature of NO₂ group weakly attached to the TNT molecule, and due the use of ultrashort pulses in a low repetition rate. For these reasons, the kinetic energy distribution obtained for NO_x fragments from TNT, do not follow the Maxwell-Boltzmann distribution, which are consistent with photothermal processes^{16,22}.

5. CONCLUSIONS AND FUTURE WORK

Femtosecond laser pulses and quadrupole mass spectroscopy measurements of have been employed to study the femtochemistry and energy distribution in solid 2,4,6-trinitrotoluene. The work was performed using 100 fs laser pulses with wavelengths of 266 nm and 400 nm. The data showed in the mass spectra, high mass fragment ions, as well as the characteristic NO and NO₂ fragments, revealing a low fragmentation degree upon ultrashort pulses photolysis. In addition, the kinetic energy distribution curves, for NO and NO₂ demonstrate the strong influence of nitro groups in the fragmentation process, suggesting the formation of NO, -the strongest signal observed- and, confirming the multiphoton character of the process. That fact is supported on the basis, that the neutral NO is formed by different ways²³, among those, the most likely to occur is the second fragmentation of nascent NO₂, formed in the photofragmentation of TNT crystals, either neat TNT or TNT on sand. Additionally, the photodissociation channels of TNT molecule results in a broad kinetic energy distribution of for NO₂ and NO, probably reflecting multiple collisions as these products exit bulk TNT crystals. The non exponential nature of the power dependence curve reflects the photochemical nature of the process presented in this thesis.

In summary, the photo-fragmentation followed by mass spectrometry measurements is a good approach for the establishment of the kinetic energy distribution of released fragments

of explosives material that contain the NO_2 group; and for future work, could be applied joined with other spectroscopic techniques for detecting different kind of explosives.

REFERENCES

1. Huber J.R.; "Photodissociation of molecules: the microscopic path of a molecular decay." *Pure & Appl. Chem.*, **1988**, *60*, 947-952
2. Fang, X.; Ledingham, K. W. D.; Graham P.; Smith, D. J.; McCanny, T.; Singhal, R. P.; Langley, A.J.; Taday, P. F. "Uniform Molecular Analysis Femtosecond Laser Mass Spectrometry." *Science-Astra Laser Programme, CLF annual Report*. **1998/1999**, 85-88.
3. Cabalo, J.; Sausa, R. "Trace detection of explosives with low vapor emissions by laser surface photofragmentation–fragment detection spectroscopy with an improved ionization probe." *Appl. Optics*, **2005**, *40*, 1084-1091.
4. Hankin, S.M.; Tasker, A.D.; Robson, L.; Ledingham, K.W.D.; Fang, X.; McKenna, P.; McCanny, T.; Singhal, R.P.; Kosmidis, C.; Tzallas, P.; Jaroszynski, D.A.; Jones, D.R.; Issac, R.C.; Jamison, S. "Femtosecond laser time-of-flight mass spectrometry of labile molecular analytes: laser-desorbed nitro-aromatic molecules." *Rapid Commun. Mass Spectrom.* **2002**, *16*, 111-116.
5. Hankin, S. M.; Fang, X.; Ledingham, K. W. D.; Singhal, R. P.; McCanny, T.; Robson, L.; Tasker, A.D.; Kosmidis, C.; Tzallas, P.A.; Langley, J.; Taday, P. F.; Divall, E. "Femtosecond Ionisation of Laser-Desorbed Atoms and Molecules." *Science-Astra Laser Programme, Central Laser Facility Annual Report*. **1999/2000**, 89-91.
6. Shu, J.; Bar, I.; Rosenwaks, S. "The use of rovibrationally excited NO photofragments as trace nitrocompounds indicators." *Appl. Phys. B*, **2000**, *70*, 621-625.
7. Wayne, R.P. *Principles and applications of photochemistry* New York: Oxford, **1988**.
8. Wayne, C.E.; Wayne, R.P. *Principles and applications of photochemistry* New York: Oxford, **1996**.

9. Gonzalez, A.C.; Larson, C.W.; McMillen D.F.; Golden, D.M. "[Molecular Dynamics Simulations of Energetic Solids](#)." *J. Phys. Chem.* **1985**. 89, 4809–4814.
10. Wu, D.; Singh, J. P.; Yueh, F.; Monts, D. L. "2,4,6-Trinitrotoluene detection by laser-photofragmentation-laser-induced fluorescence." *Applied Optics* .**1996**. 35,
11. Borman, S.; Dagani, R.; Rawls, R.L.; Zurer, P.S "75 years of chemical research." [Chem. & Eng. News](#), **1998**, 75th anniversary issue, pp. 39-75
12. UTI 100C Precision mass analyzer operating and service manual, UTHE TECHNOLOGY INTERNATIONAL.USA.
13. Atkins, P. *Physical Chemistry*. Fifth edition. W.H. Freeman and Company. New York **1994**. pp 13-16, 34-38.
14. hyperphysics.phy-astr.gsu.edu/.../kintem.html, accessed 03/03/2006.
15. J. Yinon , S. Zitrin . *Modern Methods and Applications in Analysis of Explosives*, John Wiley & Sons: New York, **1996**.
16. Weickhardt, C.; Tönnies, K. "Short pulse laser mass spectrometry of nitrotoluenes: ionization and fragmentation behavior." *Rapid Commun. Mass Spectrom.* **2002**, 16, 442-46.
17. Gomez, L.M.; Osorio, C.; Amman, E.; Hernandez, S.P.; Castro, M.E. "The spectroscopic fingerprint of TNT between 395 and 495 nm determined from transmission near field optical microscopy measurements." *Chemical Physics Letters*, **2006**, 422 (2-6), 313-316.
18. Matsumi, Y.; Murakami, S.; Kono, M.; Takahashi, K.; Koike, M.; Kondo, Y. " High-Sensitivity Instrument for Measuring Atmospheric NO₂." *Anal. Chem.***2001**, 73, 5485-5493

19. Castro, M. E.; Osorio, C.; Gomez, L. M.; Hernandez, S. P. “ Time-of-flight mass spectroscopy measurements of TNT and RDX on soil surfaces.” *Proceedings of SPIE* .**2005**. 5794, 803-811
20. Zhigilei, L.V.; Garrison, B.J. “Velocity Distributions of Molecules Ejected in Laser Ablation.” *Appl. Phys. Lett.* **1997**, 71 ,551-553.
21. Lippert, T.; Dickinson, J.T.; Hauer, M.; Kopitkovas, G. Langford, S.C.; Masuhara, H.;Nuyken, O.; Robert, J. Salmio, H.; Tada, T. Tomita, K.; Wokaun, A. “Influence of the irradiation wavelength on the ablation process of designed polymers.” *Appl. Surf. Sci.* **2002**, 197-198, 746-756.
22. Swayambunathan, V.;Singh, G.; Sausa, R. “Laser photofragmentation-fragment detection and pyrolysis-laser-induced fluorescence studies on energetic materials.” *Appl. Optics*, **1999**, 38, 6447-6454.
23. Arusi-Parpar, T.; Heflinger, D.; Lavi, R. “ Photodissociation followed by laser-induced fluorescence at atmospheric pressure and 24 °C: a unique scheme for remote detection of explosives.” *Appl. Optics*, **2001**, 36, 6677-6681.